Metamorphosed and partially molten hydrothermal alteration zones of the Akulleq glacier area, Paamiut gold province, South-West Greenland

Magnus Asiboh Tebi

Dissertations in Geology at Lund University,
Master's thesis, no 292
(45 hp/ECTS credits)

Department of Earth- and Ecosystem Sciences
Division of Geology
Lund University
2011

Metamorphosed and partially molten hydrothermal alteration zones of the Akulleq glacier area, Paamut gold province, South-West Greenland

Master's thesis

Tebi Magnus Asiboh

Department of Earth and Ecosystem Sciences
Division of Geology
Lund University

2011

Contents

Cover Picture: Field picture of metamorphosed hydrothermal alteration zone and quartz vein.

Metamorphosed and partially molten hydrothermal alteration zones of the Akulleq glacier area, Paamiut gold province, South-West Greenland

MAGNUS ASIBOH TEBI

Tebi, M., 2011: Metamorphosed and partially molten hydrothermal alteration zones of the Akulleq glacier area, Paamiut gold province, South-West Greenland. *Dissertations in Geology at Lund University, Master`s Thesis, No. 292, 26 pp. 45hskp/ECTs.*

Abstract: The Akulleq glacier area is located to the east of Paamiut settlement, South-West Greenland. Tonalite-trondhjemite- granodiorite (TTG) gneiss constitute the main rock type with an approximately 1 km wide, horse-shoe shaped supracrustal belt situated within the TTG gneiss. Meta- ultramafic lithologies form lenses in the supracrustal belt and pegmatites intruded the different lithologies. Quartz veins occur in the lenses of meta-gabbro, meta-ultramafic rock and supracrustal rocks and at their contacts with TTG gneisses. The meta-mafic rocks (meta-gabbro and amphibolite) are medium-grained and comprising hornblende, plagioclase and quartz. The abundance of quartz in meta-gabbro is higher and relict clinopyroxene is observed in places. The rocks contain cm-scale, coarse-grained leucocratic pockets, composed of plagioclase, quartz, ±orthopyroxene and clinopyroxene, which are inter-preted as *in situ* melt pockets. The elongation of hornblende characterizes a foliation in these rocks. The *in situ* pockets are parallel to the foliation and have been metamorphosed at eclogite facies conditions.

A hydrothermal alteration halo commonly surrounds quartz veins in basement rocks from NNN. Alteration assemblages vary with the rock type, but typical assemblages in meta-gabbro contains epidote, sericite, quartz, titanite, amphibole, ±biotite, ±clinozoisite and ±K-feldspar. Sulfides are pyrite, chalcopyrite, pentlandite, arsenopyrite and pyrrhotite. In felsic rocks, quartz, calcite, chlorite, K-feldspar, pyrite, chalcopyrite and pyrrhotite alteration assemblages are observed. These mineral assemblages form granoblastic quartzo-feldspathic veins and pockets that are interpreted as representing partial melt features. These leucocratic pockets are enriched in Au, containing between 100 and 400 ppb. Textural features indicate that mineralization is associated with sericitization and predates partial melting. This suggests that Au was probably remobilized into melt pockets during partial melting.

Keywords: Paamiut gold province, South-West Greenland, remobilized gold, hydrothermal alteration, sulfide.

Magnus Asiboh Tebi, Department of Earth and Ecosystem Sciences, Division of Geology, Lund University, Sölvegatan 12, SE-223 62 Lund, Sweden. E-mail: tasiboh@yahoo.com

Metamorfa och delvis smälta hydrotermala omvandlingszoner i området kring glaciären Akulleq, guldprovinsen Paamiut, sydvästra Grönland

MAGNUS ASIBOH TEBI

Tebi, M, 2011: Metamorphosed and partially molten hydrothermal alteration zones of the Akulleq glacier area, Paamiut gold province, South- West Greenland. *Examensarbeten i geologi vid Lunds universitet, Nr. 292, 26 sid. 45 hskp (45 ECTS credits).*

Sammanfattning: Området kring akulleqglaciären ligger i närheten av bosättningen Paamiut, sydvästra Grönland. Tonalit- trondhjemit och granodioritgnejser (TTG) utgör huvudlitologin i området. Inom TTG-gnejserna återfinns ett cirka 1 km brett hästskoformat bälte av suprakrustala bergarter. Ultramafiska metamorfa bergarter utgör linser i det suprakrustala bältet och pegamtiter intruderar de olika litologierna (Kolb, 2011). Kvartsådror förekommer i de ovan beskrivna linserna samt i kontakter mellan dessa och TTG-gnejserna (Kolb, 2011). De metamorfa mafiska bergarterna (metagabbro och amfibolit) har medelkornstorlek och innehåller hornblende, plagioklas och kvarts. Kvartshalten är högre i metagabbron än amfiboliten och relikt klinopyroxen är förekommande. Bergarterna innehåller cm-stora, grovkorniga, leukokratiska fickor som består av plagioklas, kvarts, ± ortopyroxen samt klinopryoxen. Dessa fickor tolkas vara bildade in situ.

Kvartsådrorna är vanligtvis omgivna av hydrotermala omvandlingshaloer. Mineralsammansättningen i de omvandlade zonerna varierar mellan olika bergarter. Omvandlad metagabbro uppvisar epidot-serisit-kvarts-titanit ± biotit ± klinozoisit ± kalifältspat-amfibol-pyrit-kalkopyrit-pentlandit-arsenopyrit-pyrrhotit-sammansättning. Omvandlade felsiska bergarter uppvisar en sammansättning bestående av kvarts, kalcit, klorit, kalifältspat, saussurit, pyrit, kalkopyrit samt pyrrhotit. Partiell uppsmältning kan i vissa fall observeras i de omvandlade zonerna, där de tidigare nämnda mineralsammansättningarna bildar granoblastiska kvartsfältspatiska, åderlika morfologier. Sulfider är i huvudsak spridda inom mesosomen, med under 1 % inom det kvartsfältspatiska lagret. De hydrotermala omvandlingszonerna är anrikade vad gäller hydratmineral. Därav kan det antagas att dessa lager har varit utsatta för uppsmältning i en högre utsträckning under progradmetamorfos, jämfört icke omvandlade bergarter i området.

Nyckelord: Paamiut guldprovins, sydvästra Grönland, hydrotermal omvandling, sulfid

Magnus Asiboh Tebi , Institutionen för geo– och ekosystemvetenskaper, Enheten för geologi, Lunds Universitet, Sölvegatan 12, 223 62 Lund, Sverige. E-post: tasiboh@yahoo.com

1. Introduction

It has long been recognized that metamorphism and deformation result in the mobilization or remobilization of sulfide ore bodies (Ramdohr 1953). Minor elements such as Ag, As, Au and Sb, have commonly been remobilized and concentrated into discrete pockets in massive sulfide deposits that have undergone metamorphism at or above the mid-amphibolite facies (Frost et al. 2002). Two genetic models i.e the crustal continuum model by Groves et al. (1992) and the metamorphic devolatilization model by Phillips & Powell (2010) have been proposed for the formation of orogenic gold and related deposits in Archean rocks.

According to Groves (1992), such deposits represent a crustal continuum that formed under a variety of crustal regimes over at least a 15 km crustal profile at PT conditions ranging from 180$^{\Theta}$C to 700$^{\Theta}$C at 5 kbar and show a corresponding variation in structural style of mineralization, vein texture, and mineralogy of wall rock alteration. The continuum model has been one of the more widely advocated genetic models for "gold only" deposits such as those found in the Archean greenstone belts (Phillips & Powell 2009). The metamorphic devolatilization model invokes a rock-dominated source process in which auriferous fluid is generated through mineral transformation on a grain-by-grain scale throughout cubic kilometers of rock mass (Phillips & Powell 2010).

Recently, the crustal continuum model for orogenic gold deposits has been discussed, mainly questioning the existence of the high temperature (hypozonal) end (Phillips & Powell 2009; Tomkins & Grundy 2009). A major gold-forming hydrothermal event at the peak of high-grade metamorphism (as implied by the continuum model) is incompatible with the partial melting of wall rock: instead of forming a hydrothermal gold deposit, an aqueous fluid introduced during partial melting would be consumed to produce further melts (Phillips & Powell 2009). A maximum temperature of approximately 550-650$^{\Theta}$C is suggested based on the facts that: 1) metamorphic devolatilization, providing the ore fluids, is most effective in the range of 440-520 $^{\Theta}$C Phillips & Powell 2010): and 2) partial melting of the hydrothermal alteration zones would start at approximately 650$^{\Theta}$C (Tomkins & Grundy 2009).

Here, I investigate auriferous rocks from the granulite facies area of the Paamiut gold province where metamorphosed gold-quartz veins that show in situ partial melting textures of hydrothermal alteration zones. The main objective of this study is to shed more light on the question whether gold is mobilized by sulfide melt during prograde metamorphism. The outlined work has three principal objectives:

1. To describe the petrography of the gold mineralization.
2. To characterize the conditions of the metamorphic overprint.
3. To develop a model for partial melt formation in the hydrothermal alteration zones.

This project is incorporated in a larger study of gold occurrences in Western Greenland by the Geological Survey of Denmark and Greenland (GEUS) financed by GEUS and the Bureau of Minerals and Petroleum, Nuuk, Greenland. Field observations and descriptions are mainly based on the report made by GEUS during the June 2010 expedition to the area of study

2. Geological setting

2.1 Regional Geology

The Paamiut gold province is situated in the southern part of the North Atlantic Craton (NAC) of South-West Greenland. Based on differences in metamorphic grade the area is divided into four different blocks (Friend & Nutman 2001; McGregor & Friend 1997), from north to south: 1) the largely granulite facies Sioraq block; 2) the amphibolite facies Paamiut block; 3) the Neria block that is totally retrogressed from the granulite facies; and 4) the low metamorphic Sermiligaarsuk block comprising the volcano-sedimentary Tartoq group. The NAC largely consist of Mesoarchean (ca. 3075-2820 Ma) orthogneisses with tonalite-trondhjemite-granodiorite (TTG) compositions (Steenfelt et al. 2005). The gneisses contain km–thick metavolcanic amphibolite layers typically bordered by km-thick layers containing anorthosite (Windley & Garde 2008). Investigation principally based on field relationship suggests that the TTG-gneisses are younger than the amphibolite (Friend & Nutman 2001). The metavolcanic belts commonly contain distinctive and diagnostic pillow-bearing basalt, tuff, pyroclastic and andesitic rocks suggesting that an arc origin is common (Windley & Garde 2008).

2.2 Local geology

The study area is situated in the Paamiut block. An approximately 1 Km wide, horse shaped supracrustal belt is situated within TTG gneiss. Meta–ultramafic lithologies form lenses in the supracrustal belt, and pegmatites intruded the different lithologies (Kolb 2011). The structure of the area is characterized by broadly north-south trending D_2 thrust zones that dip moderately to the east (Fig. 2a). Between the thrust zones earlier D_1 fabrics are preserved being variably reactivated during the later D_2, resulting in a complex interference pattern. In the foot wall of a D_2 thrust, sigmoidal S_1 dominates and indicates reverse sense of movement (Fig. 2b). The early S_1 foliation is mainly preserved in meta-gabbro, meta-ultramafic rocks and TTG gneiss (Kolb 2011).

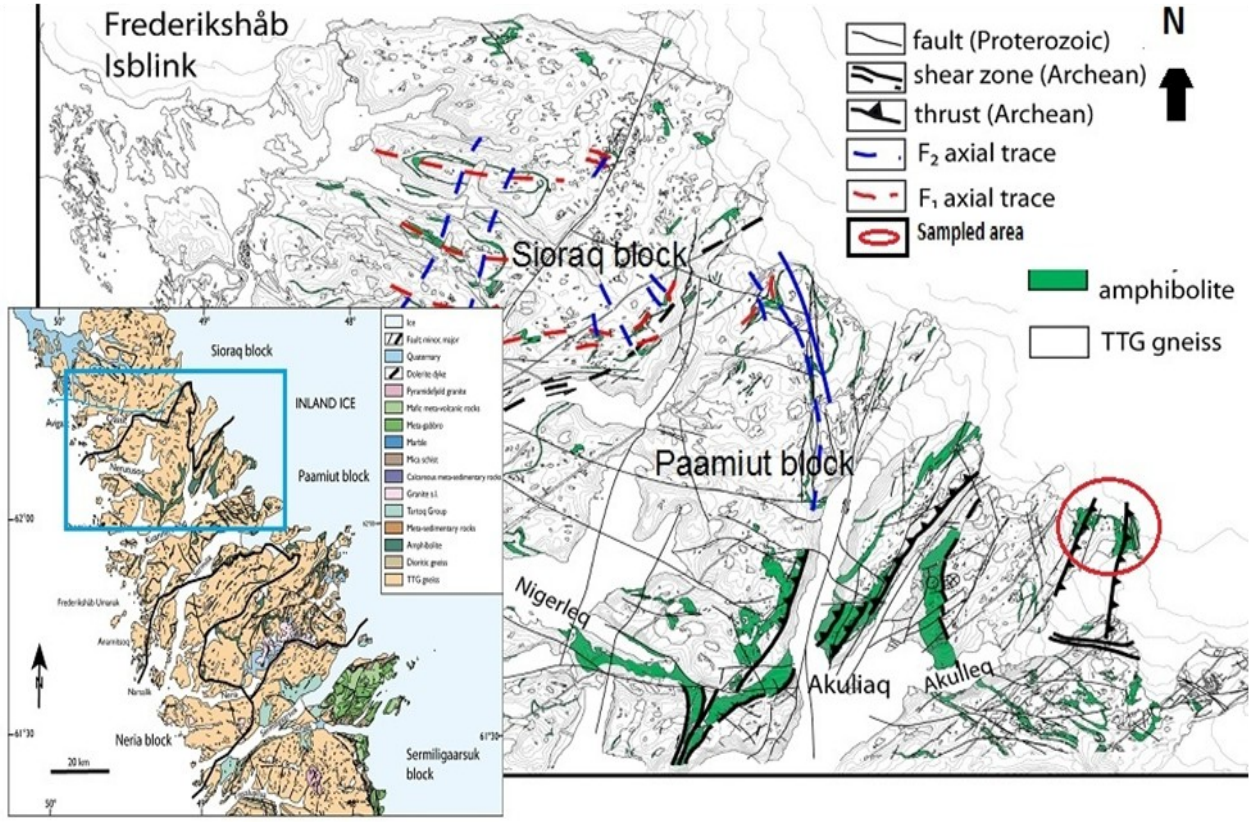

Fig. 1. Schematic geological map of South-West Greenland superimposed on the map of Sioraq and Paamiut blocks. Modified from Kolb (2011).

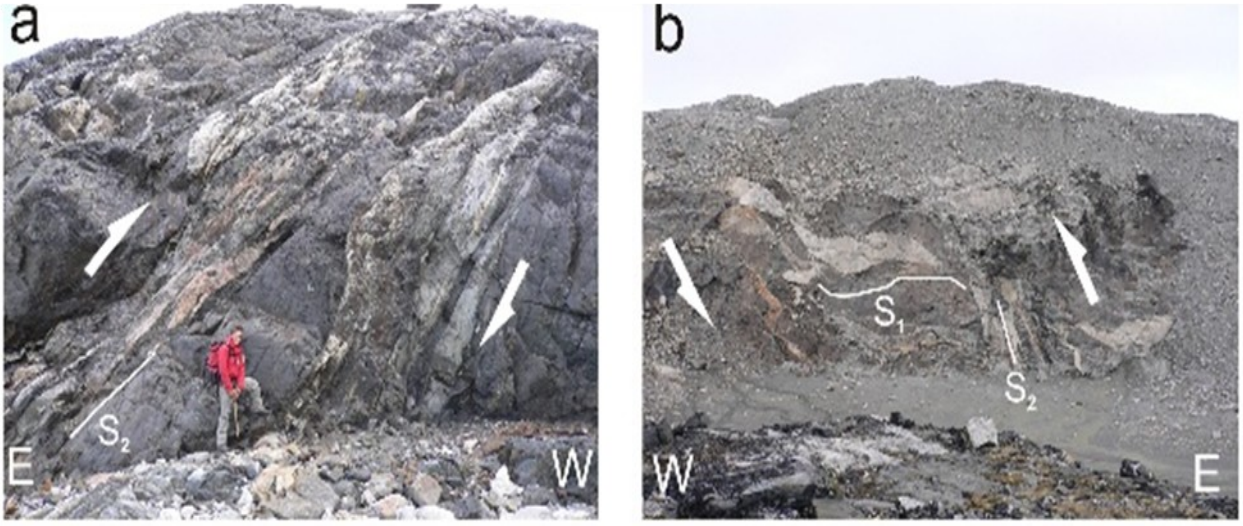

Fig. 2. **A.** Lenses of meta-ultramafic rocks form lenses in duplex structures of the west-vergent thrust. Leuco-granite intruded syn-tectonically parallel to the S_2 foliation (from Kolb, 2011). **B**. In the foot wall of a D_2 thrust, sigmoidal S_1 dominates and indicates reverse sense of movement. Note that the leuco-granite intruded parallel to S_2 , but also parallel to reactivated S_1(from Kolb, 2011).

3. Methods

A detailed petrographic study was carried out on twenty-eight thin sections and their corresponding rock samples at Lund University and GEUS.

Firstly, all thin sections were examined using a polarizing microscope fitted with x5, x10 and x40 objectives (Fig. 3a). A scan on each slide was made in order to examine different grains of unknown minerals. Color, relief, grain size, cleavage, texture, alteration, interference figures, crystal shape and birefringence were documented. These properties together with mineral identification tables were used to identify unknown minerals. Transmitted light was used to investigate silicate minerals. Ore minerals were analyzed using reflected light in air and immersion oil. Immersion oil was used to provide a better connective medium between the samples and the oil-immersion lens, thus, high resolution images for better interpretations. Ore microscopy using oil immersion was done at GEUS. Rock samples were investigated with unaided eyes and a hand lens (x10).

Secondly, five thin sections were chosen from the initial 28 samples based on the level of mineralization and alteration for investigation with scanning electron microscope (SEM: using a Hitachi S3400N fitted with an EDS (energy dispersive X-ray spectrocoscopy) detector at the Department of Earth and Ecosystem Sciences, Lund university). The SEM (Fig. 3b) was mainly used for semi-quantitative analysis i.e. to study mineral intergrowth and to produce backscattered electron images. An acceleration voltage of 15 kV was used on polished and carbon coated samples to analyze for silicates while 17.5 kV was used to carry out analysis on sulfides and oxides. A cobalt standard was used for standardization. Each spectrum was acquired for 40 seconds.

Three out of the five samples were analyzed using the electron probe microanalyzer (Fig. 3c). This analysis was conducted at the Geological Institute of the University of Copenhagen, Denmark, using a JOEL JXA-8200 WD/ED operating at a voltage 15 keV, a current of 15 nA, with 10 µm beam resolution and a wavelength dispersion (WD) length of 11 mm. Each spectrum was acquired for approximately 25 seconds. Standard reference materials were used to calibrate the instrument for quantitative analysis of plagioclase, hornblende, pyroxene, garnet and epidote. The instrument was calibrated for the following elements: Si, Fe, K, Ti, Mg, Al, Mn, Ca, and Na. The EPMA was used for quantitative analysis in order to obtain compositional data that was used for P-T estimation and calculation of mineral formula. The calculation of mineral formula was done using Andy Tindle`s mineral recalculation software Tindle & Webb (1994).

Pressure and temperature conditions were modeled using PERPLE_X version 6.6.6, source updated 8/13/2011. PERPLE_X 6.6.6 is a collection of FORTRAN 77 programs and is an automated strategy for calculation of phase diagram sections and retrieval of rock properties as a function of physical conditions (Connolly & Petrini 2002). The sub program BUILD (Appendixes 1 & 2) was used for problem definition. Equilibria reactions were calculated using subprogram VERTEX. The subprogram PSSECT was used to plot the output file from VERTEX.

The results and Interpretations of this study are based on observed metamorphic/reaction textures, chemical composition, modal abundance and distribution of minerals in thin sections and hand specimens. Pressure and temperature of peak metamorphism are modeled using the PERPLEX 6.6.6 software in order to characterize the conditions at which the gold occurrence was metamorphosed.

Fig. 3. **A.** Optical microscope. **B**. Scanning electron microscope. **C**. Electron probe micro-analyzer.

4. Petrography and mineralogy

Petrography is described in terms of wall rock and mineralization. Mineralized samples include: 517850, 517851, 517853, 517855 and 517856. Generally, plagioclase is partly or completely altered to sericite in these samples. Sample 517855 contains a distinctive quartzo-feldspathic vein. Sample 517844, 517853 contains leucocratic pockets that are parallel to a weak foliation and contain a lesser amount of sulfides. Leucocratic pockets are present in wall rock as well (sample 517865).

4.1 Wallrock

Wall rock refers to the rock that has been unaffected by mineralization and alteration. The following rock types are described: ampbibolite, meta-gabbro, pegmatites, meta-dacite, meta-dunite and meta-peridotite.

4.1.1 Amphibolite (517847, 517865)

The rock is dark-grey in colour. Generally, the rock is foliated, fine-to-medium-grained comprising hornblende (65-75%), plagioclase (5-10%), quartz (<5%) and sphene (<1%). Hornblende is elongated (Fig. 4b), medium-grained (400 µm) and characterize a foliation in the rock. Plagioclase is fine-grained, subhedral-anhedral and usually contains albite twins. Optical zonation and a black dusty alteration are observed in some plagioclase grains. Quartz is usually very fine-grained and rounded. Both quartz and plagioclase fills interstitial space between hornblende grains.

A medium to coarse-grained leucocratic part comprising clinopyroxene, orthopyroxene, quartz, plagioclase, hornblende and titanite is observed in sample 517865. The mineral grains do not show any preferred orientation. Hornblende is being replaced by clinopyroxene (Fig. 4c). The leucratic part is dominantly composed of coarse-grained (averaging 1mm) plagioclase that shows oscillatory zonation (Fig. 4d). Both orthopyroxene and clinopyroxene are euhedral and occur in lesser amounts. Plagioclase is partly altered to epidote. Hornblende, especially grains located at the boundary between leucocratic pocket and foliation are optically zoned.

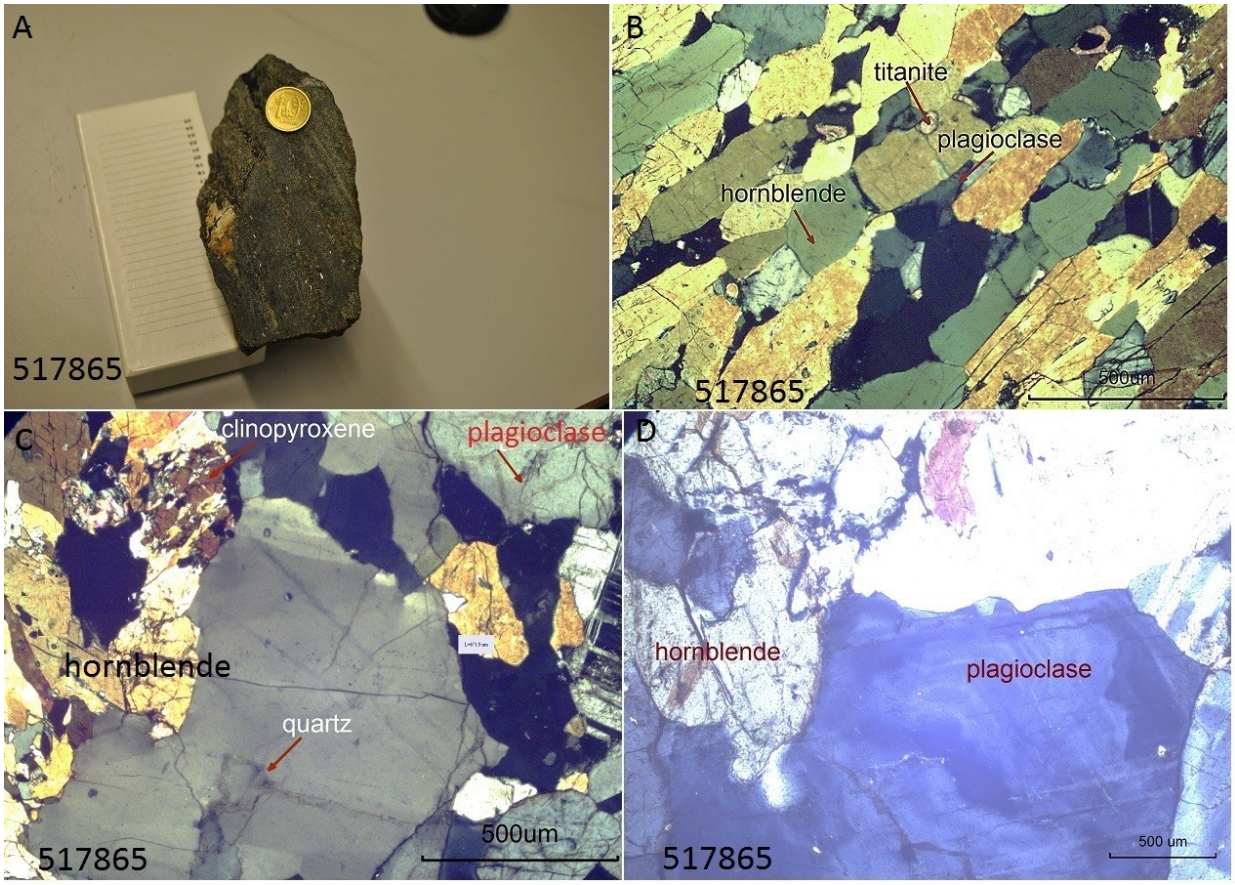

Fig. 4. **A.** Dark-grey amphibolites containing white pocket**. B**. Elongated hornblende. **C**. Replacement of hornblende by clinopyroxene. **D**. Oscillatory zoning in plagioclase.

4.1.2 Meta-gabbro (517842)

Meta-gabbros are medium-grained black-white-coloured rocks, comprising hornblende (60-75%), plagioclase (10-25%), quartz (14-20%) and clinopyroxene. The rocks contain cm-scale, coarse-grained leucocratic pockets that are composed of plagioclase, quartz and clinopyroxene . An intergrowth symplectite of epidote + quartz is observed. Fractures within the mineral grain are filled by hematite.

4.1.3 Pegmatite (517841)

The rock is white in colour and contains a dense network of fractures (Fig. 5a). It is granoblastic, coarse-grained and is consisting of plagioclase (≈45%), quartz (≈35%), K-feldspar (≈15%) and biotite (≈5%). Plagioclase is coarse-grained and can measure up to 4mm. It is antiperthertic in places and K-feldspars is partly altered to biotite (Fig. 5b). Grain boundary migration is observed in quartz mainly as bulging and nucleation.

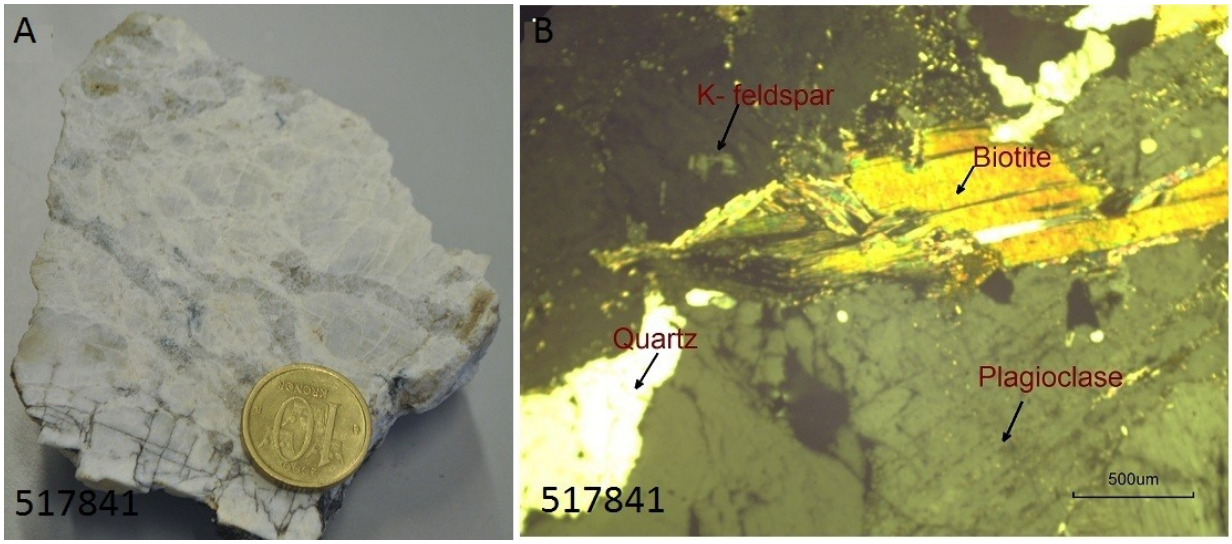

Fig. 5. **A.** Dense network of fractures in pegmatite. **B**. Alteration of plagioclase to biotite

4.1.4 Meta-dacite (517858)

Meta-dacite is buff coloured (Fig. 6a), medium-grained comprising plagioclase (≈85%), biotite (≈10%) and quartz (5%). Plagioclase occurs in blocky crystals and contains inclusions of quartz and biotite in places. Albite twinning and chemical zoning is observed in some crystals. Biotite is acicular and subhedral with an average grain size of 300 µm. It occurs mainly interstitial to plagioclase grains (Fig. 6b). The elongation of biotite defines a weak foliation in the rock. Biotite contains inclusions of zircon and a dark brown rim is observed around the zircon grains.

4.1.5 Meta-dunite (517863)

The rock is medium-grey containing greenish and white spots. It is fine to medium-grained comprising olivine (≈30%), serpentine (≈20%), amphibole (≈30%), and calcite (≈3%). Serpentine occurs as platy crystals and is seen to replace olivine. The rock shows a cumulate texture and fresh magmatic olivine is partly preserved in places (Fig. 7b). Olivine occurs as medium grained (400 µm) blocky patches in serpentine and some coarse grains as well. The patches of olivine show optical continuity. Olivine contains characteristic fractures and is being replaced by calcite and amphibole. Calcite is fine-grained (300 µm), euhedral and aggregates of calcite partly replaced serpentine. An intergrowth is observed between olivine, serpentine and amphibole.

4.1.6 Meta-peridotite (517861)

The rock is greenish in colour. It is fine to coarse-grained comprising talc (≈80%), serpentine (≈12%), clinopyroxene (≈5%) and hornblende (3%).Talc is mainly fine grained but could measure up to 500 µm. clinopyroxene is mainly subhedral with some infrequent euhedral phenocryst that have corroded edges and may reach grain size of up to 2 cm is being replaced by talc.

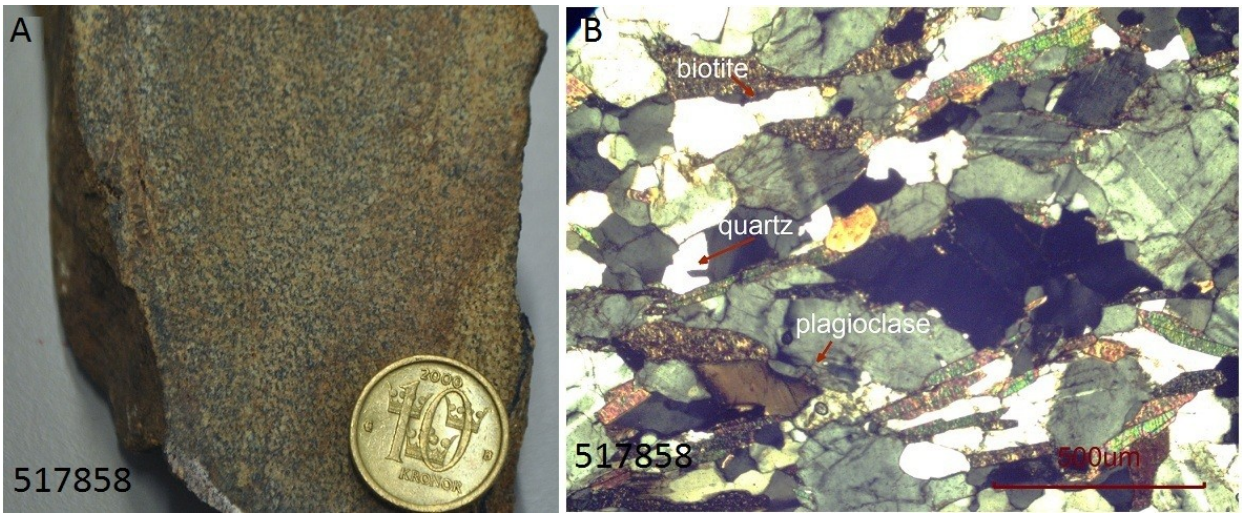

Fig.6. **A.** Buff colored meta-dacite. **B**. Interstitial biotite.

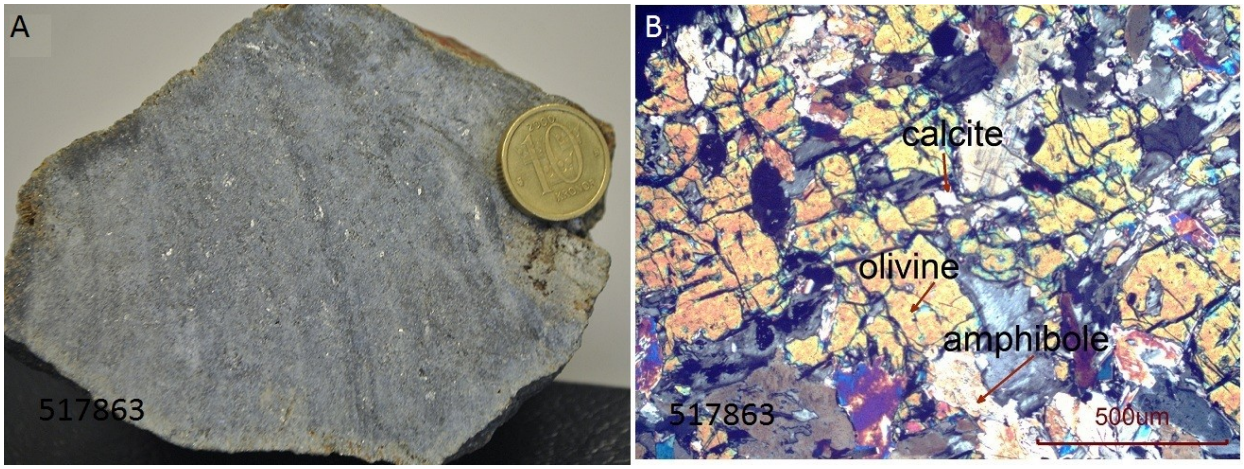

Fig. 7. **A.** Medium-grey meta-dunite containing greenish and white spots. **B.** Fresh olivine.

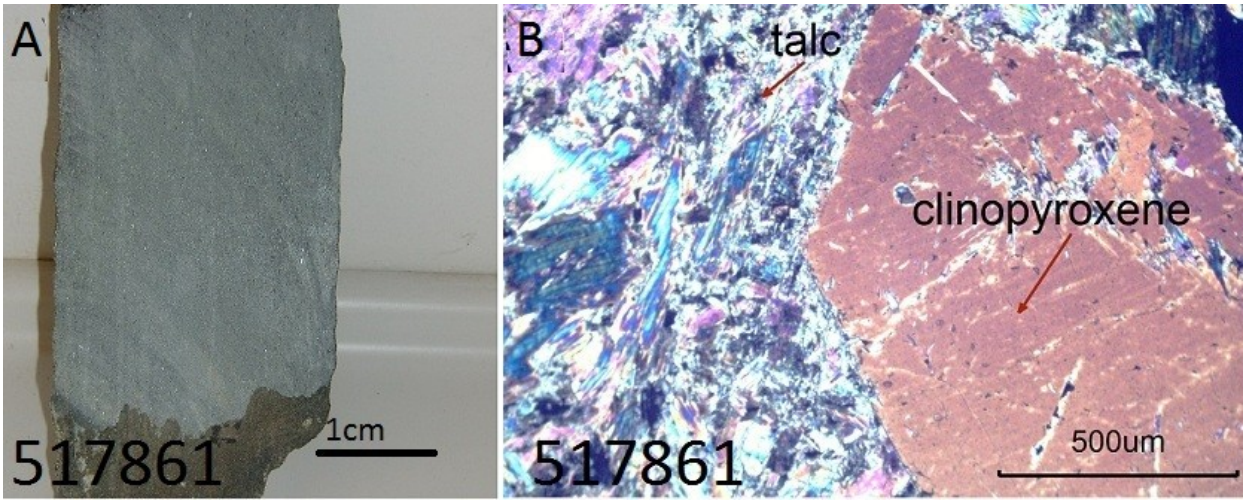

Fig. 8. **A**. Greenish meta-peridotite. **B**. Phenocryst of clinopyroxene in fine-grained matrix of talc.

4.2 Hydrothermal alteration and mineralization

4.2.1 Meta-gabbro (517850, 517851, 517855, 517856)

Sulfide mineralization occurs in the hydrothermal alteration zone. The hydrothermal alteration assemblage surrounds quartz veins and shows a rusty colour (Fig. 9a). Based on variation in modal abundance of minerals observed in sample 517855, three distinctive layers can be identified (Fig. 9b). A coarse-grained, granoblastic layer (layer 1) comprising K-feldspar (≈35%), plagioclase (≈15%), quartz (≈45%), biotite(≈3%), titanite (<1%) and sulfide (< 1%) is observed (Fig. 9c). Hematite mainly fills grain boundaries and fractures within this layer. Layer 2 is dominantly made up of coarse-grained, euhedral crystals of clinopyroxene (≈50%), plagioclase (≈5%), quartz (≈40%) and pyrite (≈2%). Clinopyroxene is unaltered and occur interstitial to quartz grains (Fig. 9d).

Layer 2 grades laterally into a fine to medium-grained assemblage and contains sericite (≈45%), epidote (≈7%), sphene (≈5%), quartz (≈15%), plagioclase (≈3%), hornblende (≈10%), clinozoisite (≈3%), and clinopyroxene (<1%). Clinopyroxene is altered to amphibole (Fig. 9e). Fine-grained disseminated sulfides locally, in layer 3, reach abundance of ≈15% with the sulfide mineralogy being dominated by pyrite, pyrrhotite, chalcopyrite and pentlandite.

The mineral assemblage in layer three does not show any preferred orientation and, the layer is characterized by mm-scale quartz veins. The quartz veins have lobate grain boundaries with interstitial pyrite between quartz grains. Inclusions of pyrite are also observed in quartz grains. The average grain size in layer 3 is 200 μm which is about one-third the grain size in layer 2 and layer 1. In layer3, plagioclase occurs mainly as patchy crystals and is being partly or completely altered to sericite (Fig. 9f).

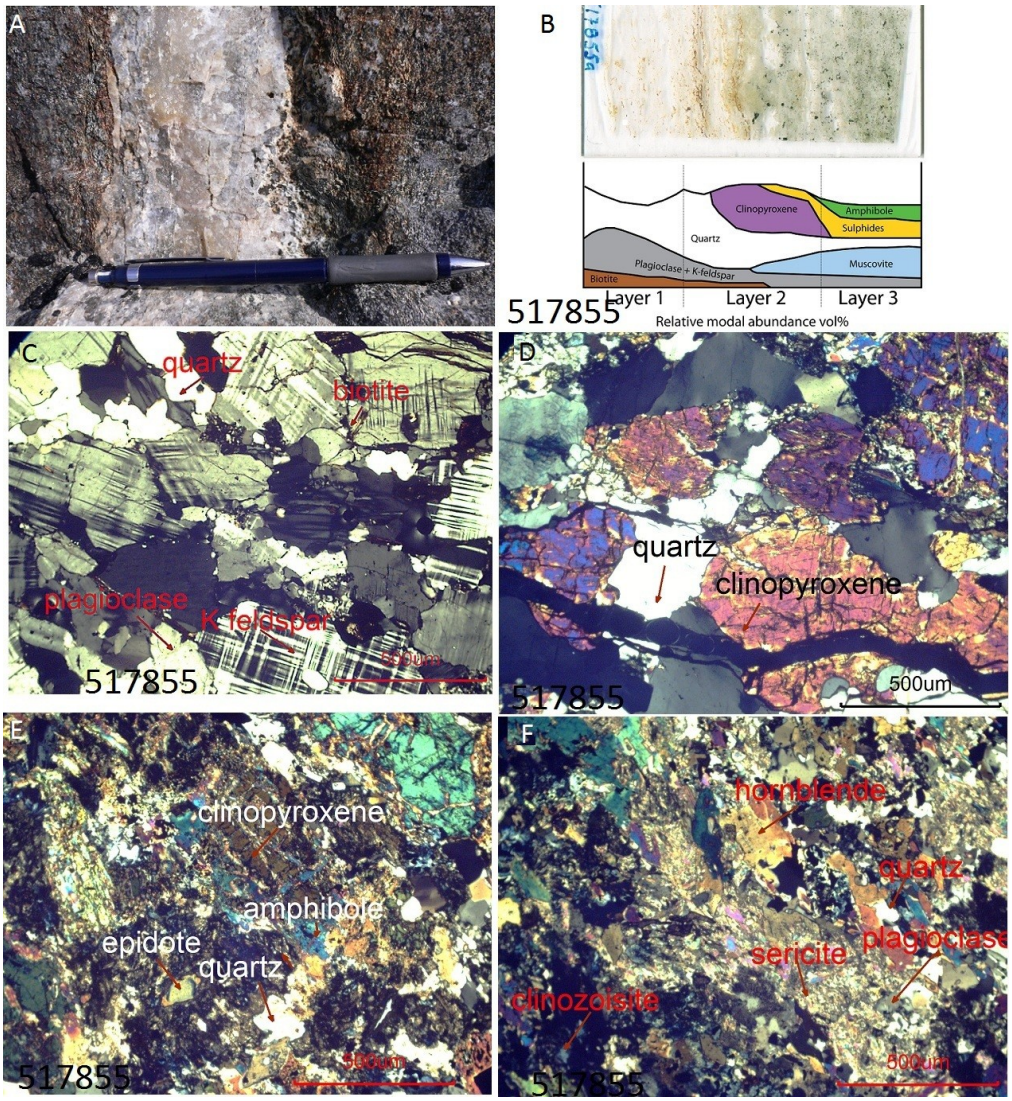

Fig. 9. **A**. Field picture of metamorphosed hydrothermal alteration zone and quartz vein**. B.** Variation in modal abundance of minerals across sample 517855. **C**. Granoblastic quartzo –feldspathic vein. **D.** Unaltered interstitial clinopyroxene. **E**. Alteration of clinopyroxene to amphibole. **F.** Fine-grained alteration assemblage of sericite, quartz and clinozoisite.

The relative abundance of sulfide varies with sample. Generally, pyrite is the most abundant sulfide observed. Pyrrhotite is subidiomorphic and usually contains inclusions of chalcopyrite (Fig.10a). Cleavage cracks are observed in pyrrhotite. Pyrite is mainly idiomorphic and three generations of pyrite are observed. The first generation occurs in isolation in the silicate matrix and usually contains inclusions of chalcopyrite. A second generation of pyrite is superimposed on pyrrhotite (Fig. 10b) and the third generation is associated with the alteration of pyrrhotite to magnetite and pyrite (Fig. 10c). Sulfides very often occur as inclusions in hematite (Fig. 10d).

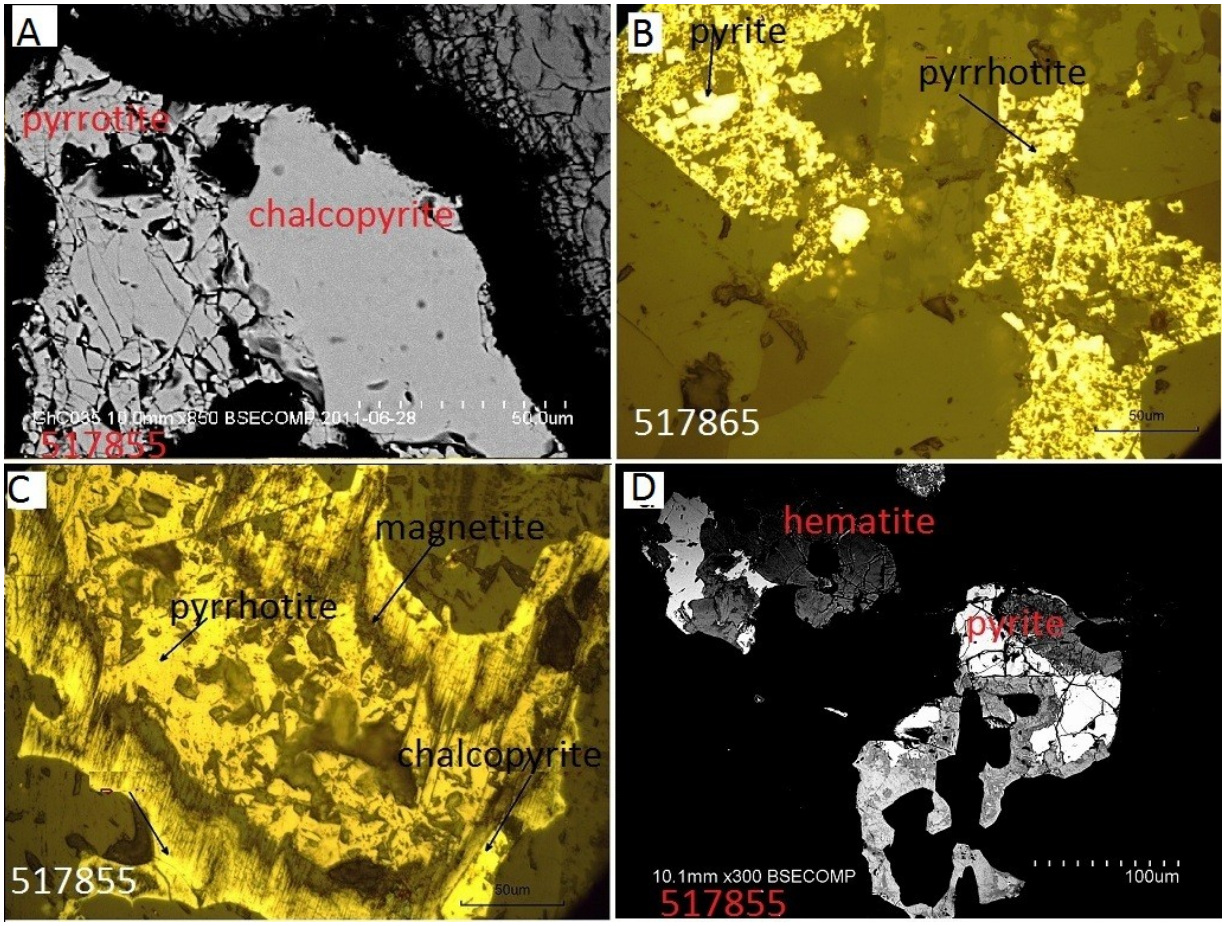

Fig. 10. **A.** Inclusion of chalcopyrite in pyrrhotite. **B**. Exsolve pyrite from pyrrhotite. **C**. Alteration of Pyrrhotite to Pyrite and

4.2.2 Amphibolite (517843, 517844, 517853,517864)

Sulfide mineralisation in amphibolite is hosted within leucocratic pockets (2-3cm wide) that lie parallel to the S1 foliation. The leucocratic pockets are dominantly medium-grained comprising clinopyroxene, hornblende, epidote, titanite, ±garnet, ±plagioclase, ± orthopyroxene, quartz, chalcopyrite, pyrite, arsenopyrite and hematite. Sulfides are mainly observed as inclusions in hematite (Fig. 10d).

The quantity of each mineral and textures observed greatly vary with sample. Generally, clinopyroxene is subhedral-anhedral and is colorless to faint green in thin sections. In garnet bearing sample (517844), hornblende and quartz occur interstitial to clinopyroxene and garnet grain boundaries (Fig. 11d). Garnet occurs as patches in hornblende and titanite forms aggregates around areas of replacement (Fig.11c). Hornblende is tabular and in addition to garnet also contains inclusion of epidote and titanite. Two generations of epidote are observed: (1) magmatic (sample 517844, 517853); and (2) retrograde (sample 517842). Magmatic epidote is idiomorphic, medium-grained and show optical zonation. Retrograde epidote is mainly anhedral and replaces amphibole (Fig.11f). A wormlike intergrowth of quartz in epidote (symplectite) is observed in sample 517853 (Fig. 11h). The symplectic intergrowth of epidote and quartz extends outwards from the retrograde epidote and invades nearby plagioclase. Titanite is medium-grained and idiomorphic.

Orthopyroxene is less common and is only observed in samples 517853 and 517864. It is medium -grained, euhedral and show first-order interference color. In sample 517842, Clinopyroxene is euhedral to subhedral, coarse-grained and is being altered to amphibole (Fig. 11g). The amphibole is faint green in color, slightly pleochroic and contains the typical amphibole cleavage. The amphibole shows sieve

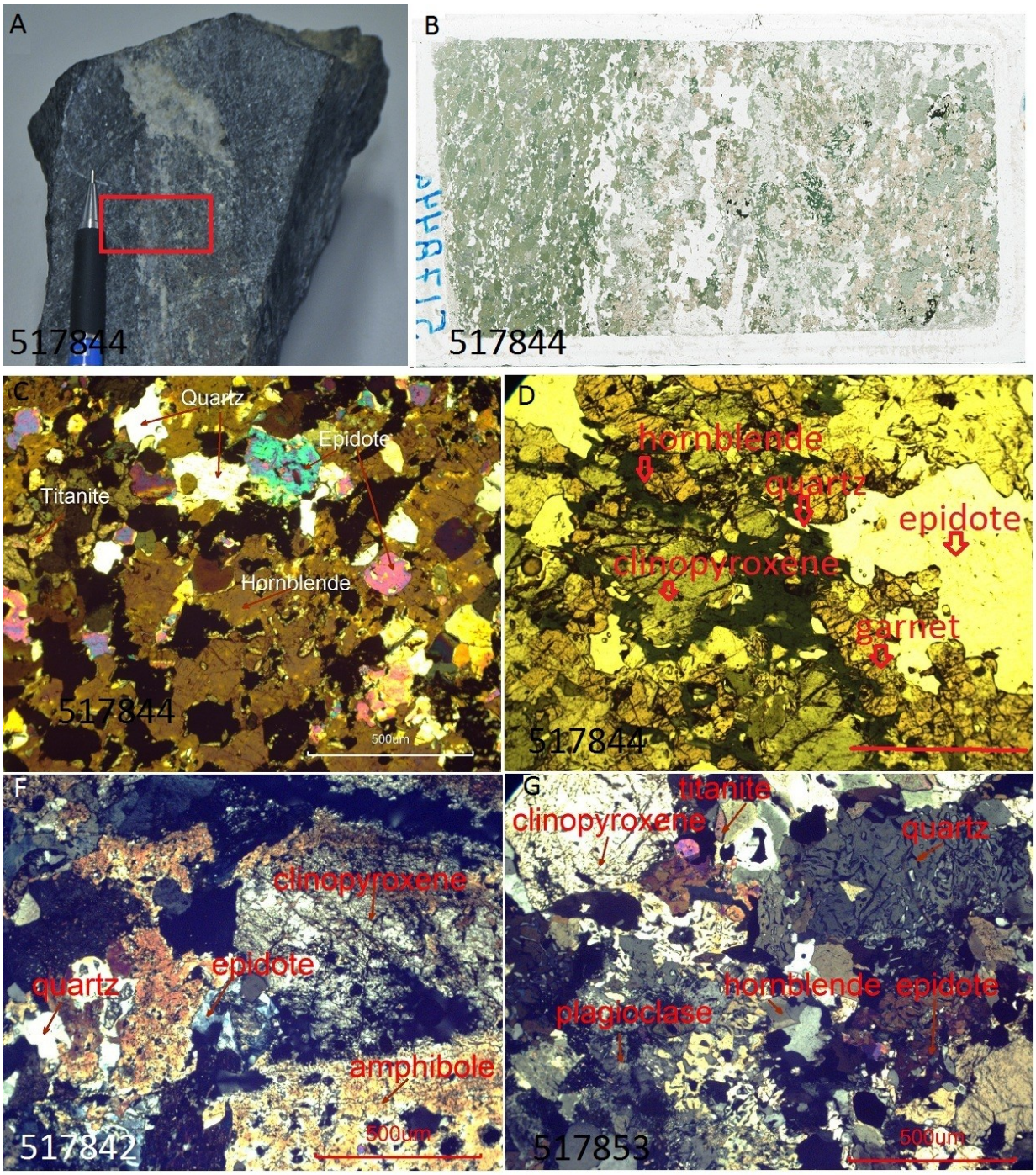

Fig. 11. **A.** Amphibolite containing leucocratic pocket. **B**. Thin section. **C**. Replacement textures showing patches of garnet in hornblende and aggregates of sphene. **D**. Reaction textures at grain boundaries between garnet and clinopyroxene. **E.** Replacement textures (amphibole = Epidote + quartz). **F**. Symplectic intergrowth of epidote and quartz.

4.2.3 Meta-dacite (517845)

The rock is fine to coarse-grained and contains a quartz vein that is approximately 1.5mm wide. Quartz is mainly coarse-grained within quartz vein. Recrystalization of fine-grained quartz that is interstitial to the coarse grains is observed. The rock is foliated and is characterized by abundant pseudomorphs after plagioclase. The hydrothermal alteration assemblage comprises saussurite (31%), chlorite (2%), epidote (<1%), K-feldspar (3%) and sphene (1%). The rock also contains hornblende (2%), plagioclase (40%), biotite (5%) and quartz (15%). Plagioclase is mainly medium-grained and is being partly or completely altered to calcite. Biotite is being altered to chlorite especially along cleavage planes.

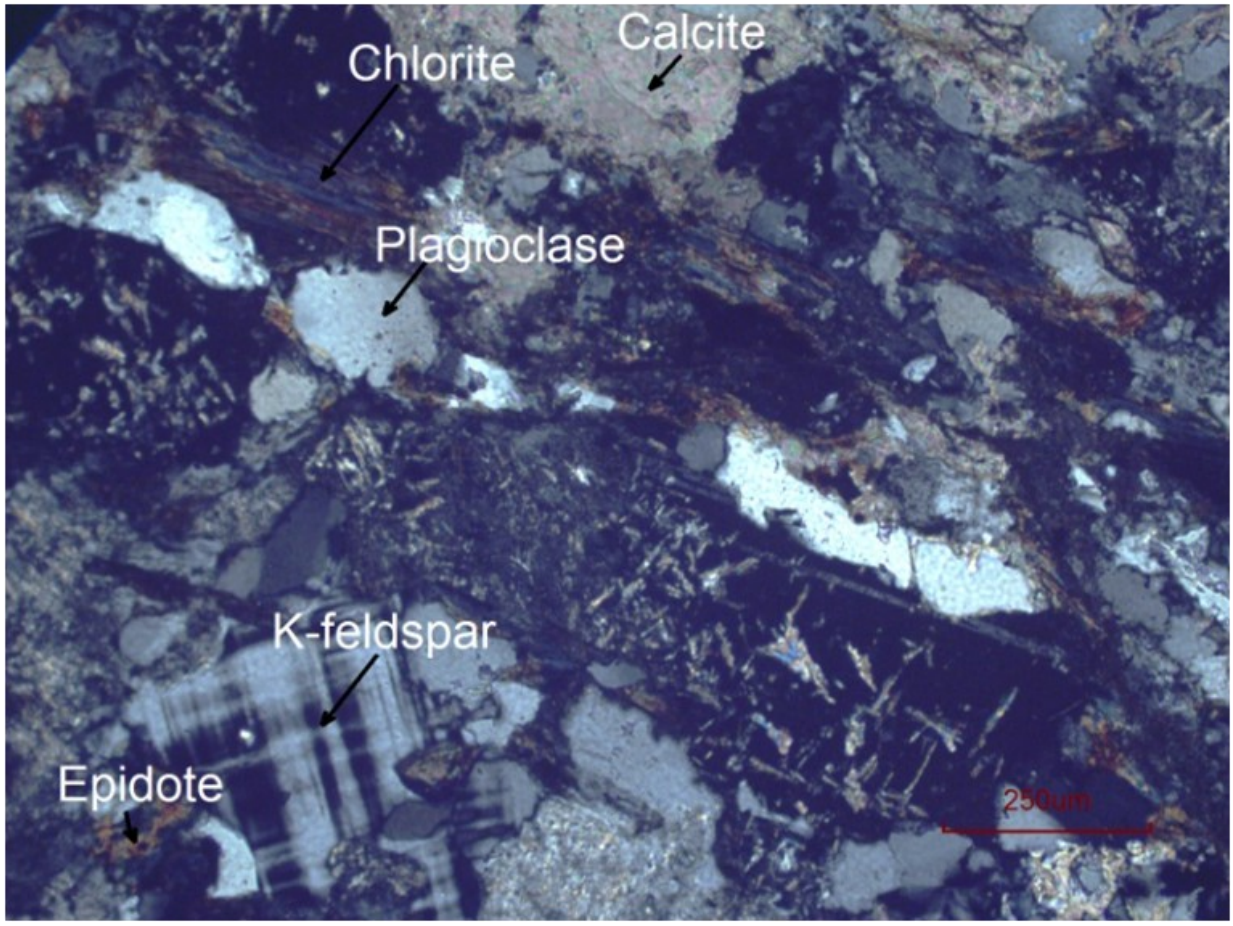

Fig. 12. Saussuritisation and alteration of biotite to chlorite in meta-dacite.

Table 1: Mineral abundance in studied sample (visual estimates)

	Peak metamorphic/magmatic assemblage										hydrothermal alteration assemblage													
sample #	Cpx	Grt	Ep	Hbl	Pl	Bt	Kfsp	Opx	Qtz	Ttn	Amph	Ep	Py	Po	Ccp	Asp	Mu	zo	Chl	Bt	Qtz	Ttn	Kfsp	Ser
Amphibolite																								
517843				85					5											10				
517844 leucocratic part	10	15	30								10		x	x	x	x						5		
517847		5		65	25				5															
517848				75	10				5			3						x	x					
517853 leucocratic part	30			10	5			5	x		5	10	x	x	x						10	x		
517864	3			60	25			x	30			3	x	x	x			x						
517865 leucocratic part	x			60	10			x	10			x												
Meta-gabbro																								
517842	x								10		60	15										x		x
517850				60	15							10	20		x	x	x				x	x	x	20
517851	3		3	65	5				3			5									10			
517852	3			60	8						3	2	x		x									
517855	x			50		x	10		30		5	x	x	x	x		x	10			20	x	x	x
517856	x						5					x					3	x		x	5			5

	Peak metamorphic/magmatic assemblage				hydrothermal alteration									
Meta-dacite	Pl	Qtz	Bt	Hbl	Pl	Qtz	Chl	Cc	Py	Ccp	Ttn	Ep		Kfsp
517845	40	20	5	5	10		x		x		x	3	x	2
517858	75	15	10						x	x				
Ultramafic rocks														
	Ol	Cpx	Bt	Amph	Di	Cc	Tlc	Srp	Amph	Mgt	Ccp	Py		
517854									98	x	x			
517861		3		5			90							
517862	3					15		10		x	x	x		
517863	50					x		30	20					

x =mineral abundance less than 1%. (Cpx =clinopyroxene, Grt =garnet, Hbl =hornblende, Pl =plagioclase, Bt = biotite, K-fsp= Potassium feldspar, Qtz =quartz, Ttn =titanite, Amp =amphibole, Ep =epidote, Po =Pyrrhotite, Ccp =chalcopyrite, empty cell =not detected)

5. Mineral chemistry

The structural formula of minerals was calculated using mineral composition obtained by WDS (Table 1). Pyroxene, garnet and plagioclase were normalized to 4, 12, 6 oxygen respectively. FeO =FeO_{total} and Fe^{3+} was recalculated based on stiochiometry and charge balance. Epidote was normalized to 12.5 oxygen and calculating FeO_{total} as Fe^{3+}. The structural formula for hornblende was calculated using PROBE-AMPH (an amphibole structural formula calculator and classifier with barometers). Hornblende was normalized based on 23 oxygens.(Tindle & Webb, 1994).

Garnet core (sample 517844) is rich in almandine (46.90%), grossular (43.39%), poor in pyrope (3.23%) and spessartine (1.59%). Garnet zoning is very faint. The garnet rim is slightly enriched in grossular (43.7%) and depleted in almandine (46.80%). Plagioclase in both sanple 517853 and hydrothermal alteration zone (sample 51855) is highly albitic with albite (72.60-92.00%), anorthite (6.26-26.62%) and orthoclase (0.50-1.02%). Pyroxene contains enstatite (30.75 - 39.94%), wollastonite (50.37 - 51.60%), ferrosillite (10.18-17.64%). The Mg# for hornblende is 0.35 and 0.45 for sample 517844 and sample 517853 respectively. The Al-content in hornblende for garnet bearing sample shows pressure of 6.5 ± 1 kbar calculated using PROBE - AMPH (Tindle & Webb, 1994). The calculated pressure based on the Al-content in non-garnet bearing sample is 4.5 ± 1Kbar.

Whole rock geochemistry (Appendix 3) shows that there is no trend in the variation of major elements distibution in studied samples. However, sample 517850 and sample 517851 are enriched in Fe_2O_3 (20.00–22.24 wt%). Sample 517855 is enriched in SiO2 (57.1 wt %) and CaO (10.00 wt%). Minor element composition shows that the following samples: 517844, 517853, 517850, 517851, 517855, 517856 are enriched in Cu (170– 1290 ppm), Au (113– 410 ppb), As (5.9 –36.0 ppm),

6. Thermobarometry

Thermobarometry is the quantitative determination of the temperature and pressure at which a metamorphic or igneous rock reached chemical equilibrium. Because pseudosections provide a map of both mineral chemistry and modes as a function of environmental variables, they have application in thermobarometry (Stuewe & Powell 1995); where, compared to conventional inverse modelling thermobarometric techniqes, phase diagram based methods have the advantage of thermodynamic consistency (Connolly et al. 1994). The main disadvantage using this method for PT evaluation is that in any natural system, there is no meaningful effective bulk composition because disequilibrium fractionation continuously modifies the composition of the rock in response to environmental factors (Connolly & Petrini 2002).

The following specifications were used to model for the formation of partial melts in the hydrothermal alteration zone: (1) thermodynamic data file from hp02ver.dat; (2) component saturation with SiO_2 ; (3) $MgO\text{-}Na_2O\text{-}K_2O\text{-}CaO\text{-}AL_2O_3\text{-}FeO\text{-}H_2O$ as thermodynamic components, (4) fluid routine 5 (Holland & Powell 1991); (5) solution models feldspar-Cpx(HP)-GlTrTsPg-pMELTS(G)-Pheng(HP) from solution model file solut.dat; (6) pressure in the range of 3000 – 8000 bar, temperature 573-1073K. The run time for a full chemical system is 20 hours and the number of pseudocompounds produced by PERPLE 6.6.6 software is so many that it makes interpretation difficult. The following components were therefore not considered TIO_2 and MnO because they occur in relatively small quantities and probably have very little effect on the stability of the mineral phases considered..

The choice of the solution models and bulk composition plays a fundamental role in determining which mineral phases are stable at any PT conditions. The pseudosection (Fig. 13) was calculated for the bulk composition of sample 517855. The results show that the formation of partial melt in a system containing amphibole, plagioclase, muscovite, quartz and clinopyroxene is strongly dependent on temperature. Partial melting will start at $600^{O}C$ regardless of the pressures. Clinopyroxene is stable over a wide range of temperatures and pressures and is the last mineral phase to be consumed. In a MnO-poor system, garnet is uncommon for pressures less than 4500 bar.

With increasing temperatures, mica is dehydrated. Amphibole is consumed, then feldspar and orthopyroxene. The model system can be used to predict the formation of partial melting formation in the hydrothermal alteration zone. However, the observed mineral composition did not plot in the model system probably because of fractionation and disequilibrium in the observed mineral assemblages.

The peak metamorphic assemblage in the garnet bearing sample (517844) plots in the eclogite field (Fig. 14). The phase compositions at 900 k and 18000 bar calculated using the subprogram MEEMUM is given below:

Mineral phases	Wt.%	Vol. %
Epidote	14.98	16.20
Garnet	58.43	54.50
Clinopyroxene	26.59	29.31

Mineral isopleths for garnet (Fig. 16) and clinopyroxene (Fig. 17) were calculated based on magnessium number, using the sub-program WERAMI and plotted using PSTABLE. The minimum contour level is represented by a solid line while the maximum value is indicated by a dotted line. Garnet isopleths are dependent on temperatures and therefore can used to estimate the temperatures at which the stable mineral phases are formed.

Table 2: Electron microprobe analysis for selected mineral phases in the hydrothermal alteration zones and in situ meltpocket in amphibolite

sample #	517844	517844	517844	517844	517853	517853	517853	517855	517855	517855
mineral	Grt	Grt	Hbl	Ep	Hbl	Cpx	Pl	Cpx	Pl	Bt
	core	rim								
wt %										
SiO2	37.4	37.1	41.8	37.4	44.4	51.3	60.2	52.1	65.4	36.0
TiO2	0.1	0.1	0.3	0.2	0.4	0.1	0.0	0.1	0.0	1.6
Al2O3	20.1	20.0	11.8	25.2	10.0	1.3	23.4	0.7	20.5	22.6
FeO	23.2	22.8	22.5	9.0	19.6	13.0	0.1	6.2	0.1	0.9
MnO	0.7	0.7	0.3	0.1	0.4	0.4	0.0	0.5	0.0	0.0
MgO	0.8	0.9	5.6	0.0	8.4	10.0	0.0	13.5	0.0	2.6
CaO	16.8	16.6	12.0	23.2	12.1	23.3	5.7	24.1	1.5	1.0
Na2O	0.1	0.1	1.4	0.1	1.6	0.6	8.8	0.4	11.5	0.2
K2O	0.1	0.1	0.4	0.1	0.4	0.1	0.2	0.3	0.1	7.7
total	99.3	98.6	96.2	95.4	97.3	100.2	98.5	98.0	99.2	71.1
no. of oxygen	12.0	12.0	23.0	12.5	23.0	6.0	8.0	6.0	8.0	11.0
Structural formulae										
Si	3.0	3.0	6.5	3.0	6.7	1.9	2.7	2.0	2.9	6.3
Al^{4+}	0.0	0.0	1.5	2.4	1.3	0.1	1.2	0.0	1.1	1.7
Al^{6+}	1.9	1.9	0.7		0.5	0.0				2.9
Ti	0.0	0.0	0.0	0.0	0.0	0.0	0.0	0.0	0.0	0.2
Cr	0.0	0.0	0.0	0.0	0.0	0.0	0.0			0.0
Fe^{3+}	0.1	0.1	0.2	0.6	0.2	0.1	0.0	0.0	0.0	1.5
Fe^{2+}	1.5	1.4	2.7	0.0	2.3	0.3	0.0	0.2	0.0	0.1
Mn	0.0	0.0	0.0	0.0	0.1	0.0	0.0	0.0	0.0	0.0
Mg	0.1	0.1	1.3	0.0	1.9	0.6	0.0	0.8		0.7
Ni	0.0	0.0	0.0	0.0	0.0	0.0	0.0			
K	0.0	0.0	0.1	0.0	0.1	0.0	0.0		0.0	1.7
Ca	1.4	1.4	2.0	2.0	2.0	0.9	0.3	1.0	0.1	0.2
Na			0.4		0.5		0.8	0.0	1.0	0.1
Total cations	8.0	8.0	17.5		17.5			4.0		
$Mg/(Mg+Fe^{2+})$			0.3		0.5					
end members										
Almandine	47.0	46.8				Wo=51.60	An=26.31	wo=50.37	An=6.52	
Andradite	4.9	4.4				En=30.75	Ab=72.66	En=39.44	Ab=92.9	
Grossular	43.4	43.7				Fs=17.64	Or=1.02	Fs=10.18	Or=0.50	
Pyrope	3.2	3.4								
Spessartine	1.6	1.6								
P (kbars)										
Hammarstrom & Zen 86			7.0		5.1					
Hollister et al. 87			7.5		5.4					
Johnson & Rutherford 89			5.7		4.1					
Schmidt 92			7.3		5.5					

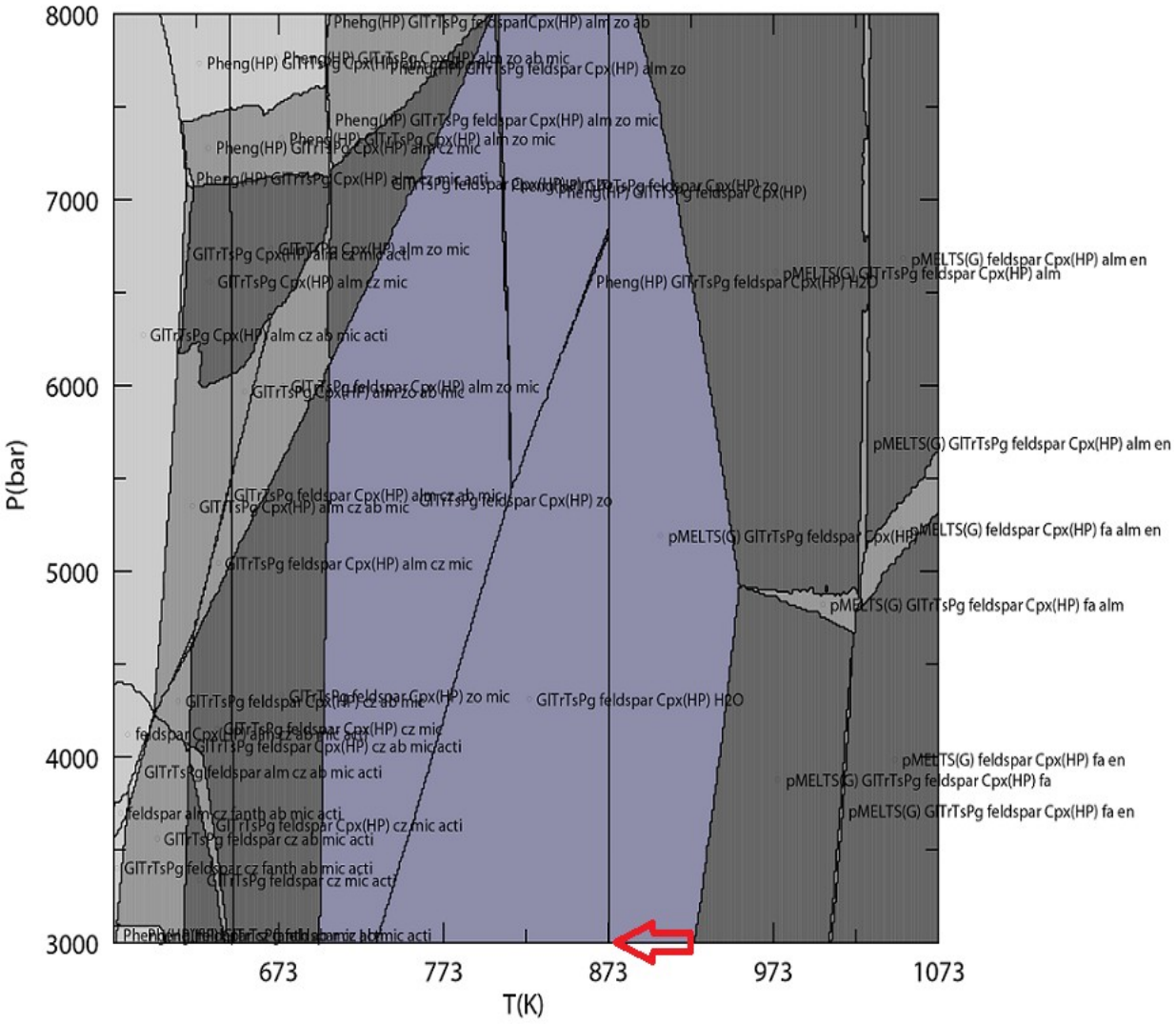

Fig. 13. A modelled P-T pseudosection using Perple_6.6.6 (Connolly 1990) for the formation of melt in the hydrothermal alteration zone calculated in the KCNFMASH system using bulk composition for sample 517855. The various colours represent the variance (GlTrTsPg = amphibole, Cpx(Hp) =clinopyroxene, Opx(HP) = orthopyroxene, mic = mica, pMELTS= melt, zo =zoisite)

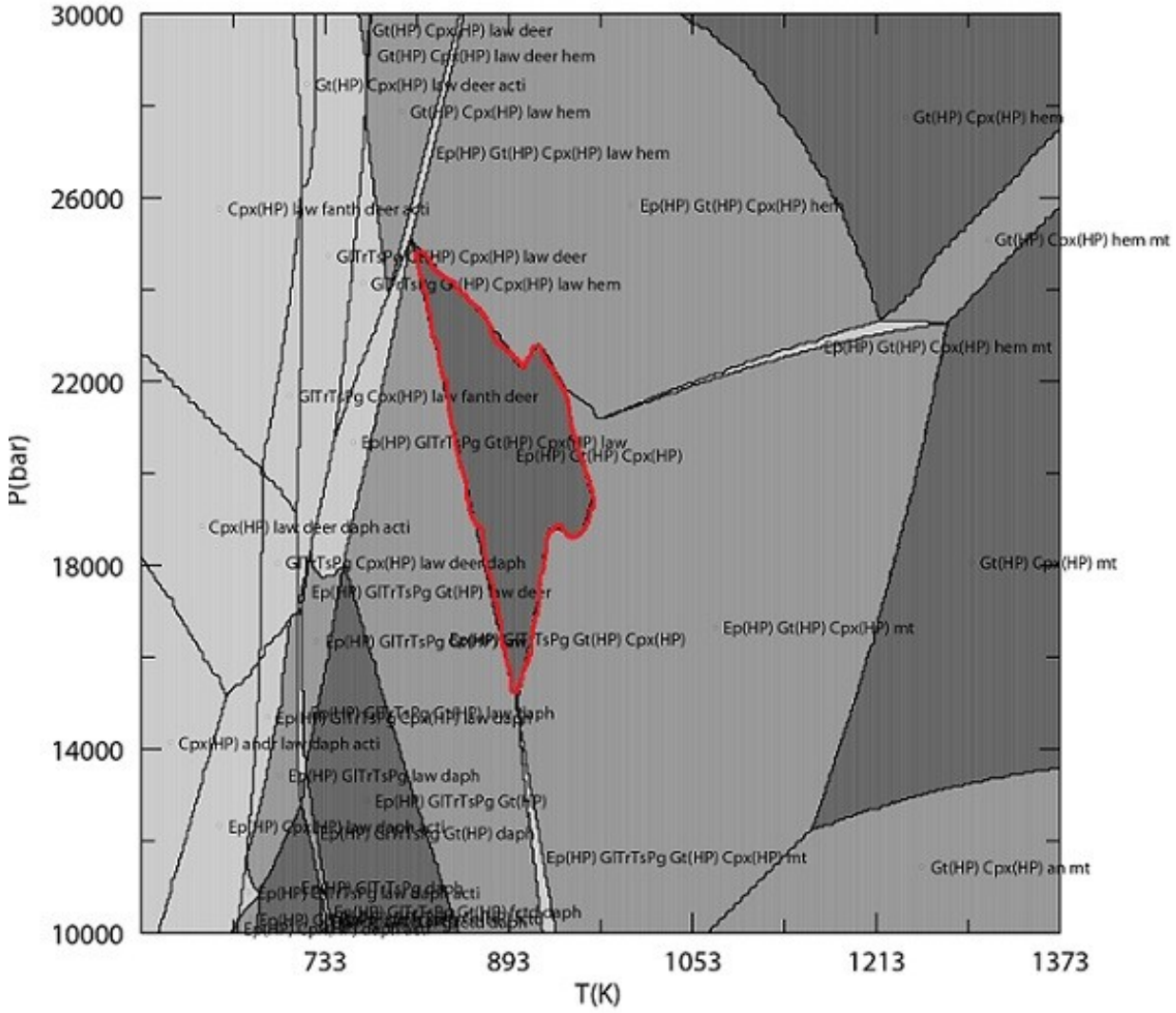

Fig. 14. A P-T pseudosection using Perple_6.6.6 (Connolly 1990) for peak metamorphic assemblage calculated using bulk composition for sample 517844. The various colours represent the variance (GlTrTsPg = amphibole, Cpx(Hp) =clinopyroxene, Gt(HP) =garnet, Ep(HP) =epidote, acti =actinolite, hem =hematiteOpx(HP) = orthopyroxene, mt =magnetite)

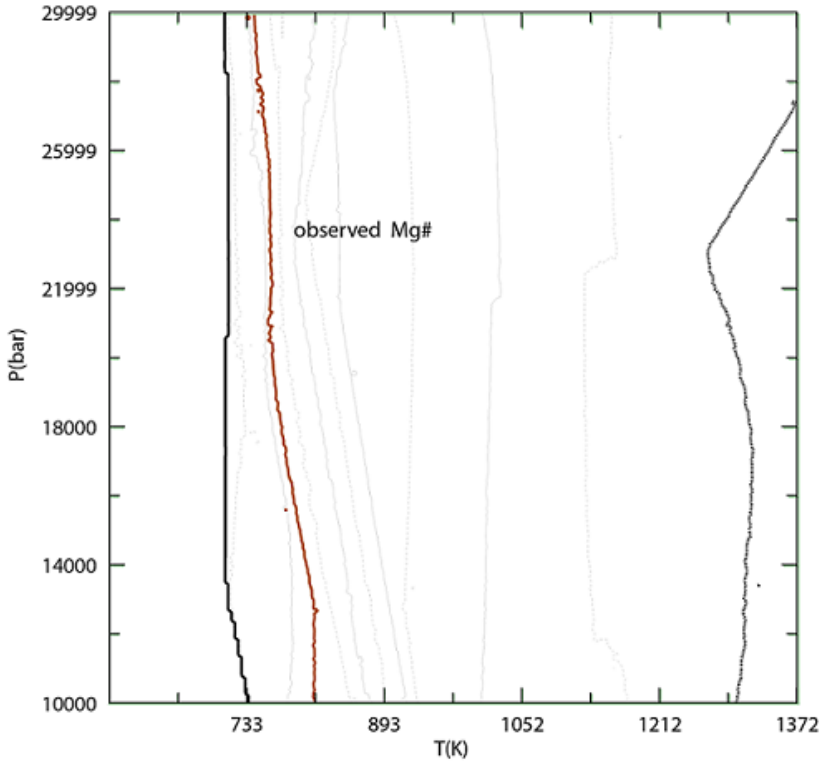

Fig. 15. Isopleths of Mg# in garnet calculated using bulk composition of sample 51744(min/max contours =thick solid/dotted curve, range =0.01-0.22, contour interval =0.07).

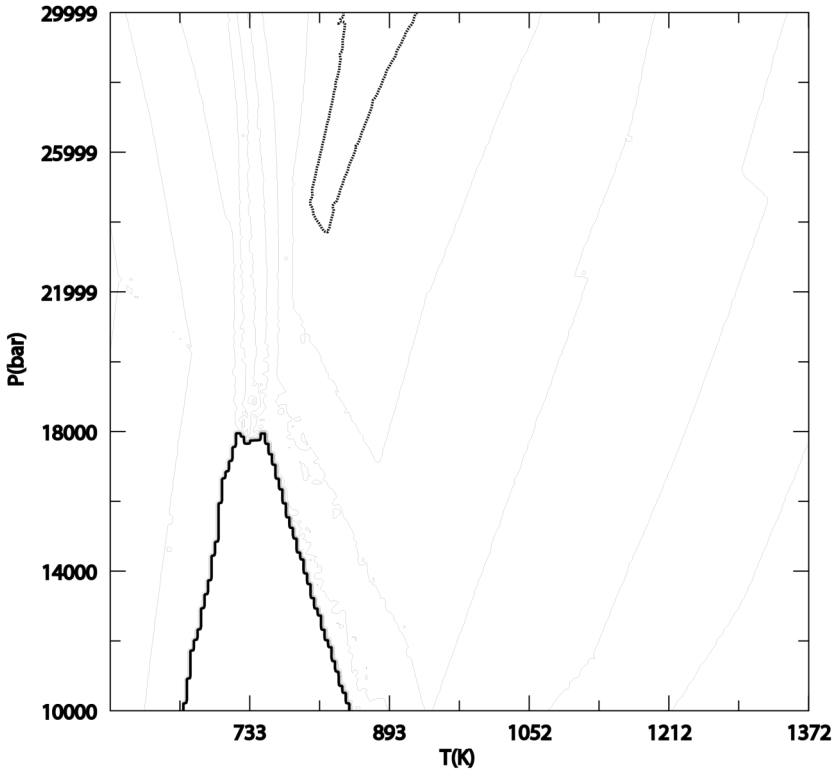

Fig. 16. Isopleths of Mg# in clinopyroxene calculated using bulk composition of sample 51744(min/max contours =thick solid/dotted curve, range =0.03-0.75, contour interval =0.07).

7. Interpretation and discussion

The textures and mineral phases contain in sample 517844 and 517853 is used for the interpretation of the metamorphic evolution in amphibolites (Table 3). The quartz-rich area (Fig. 11a) observed in sample 517844 probably represents fractionates of granitic melt. Garnet, clinopyroxene and epidote are probably residual phases. The leucocratic pockets observed in these samples are interpreted as in situ partial melt pocket. Optical zonation in epidote is interpreted as retrograde readjustment. The homogenous and the lack of low grade phase inclusions in garnet suggest a relatively late stage of garnet growth during prograde metamorphism. The absence of plagioclase and composition of garnet suggest that peak metamorphism was probably achieved under eclogite facies conditions. The in-situ melt pocket lie parallel to S_1 foliation and melt segregation is interpreted to have formed in a dynamic environment probably during D_1 deformation.

Sample 517853 contains a more or less homogenous coarse-grained assemblage. This assemblage suggests a dehydration melting of hornblende during prograde metamorphism which can expressed as:

Hornblende + quartz = clinopyroxene + orthopyroxene + plagioclase + melt.

The symplectic intergrowth of epidote and quartz (Fig.11h) in this sample suggest a retrograde reaction. A possible equation for the formation of symplectite in this sample is as follows:

Plagioclase + clinopyroxene + H2O =Epidote + hornblende + Quartz

The above reaction and the presence of titanite suggest retrogression in greenschist facies condition.

Table 3. Paragenetic table in amphibolite based on observed textures and mineralogy in sample 5178544 and 517853.

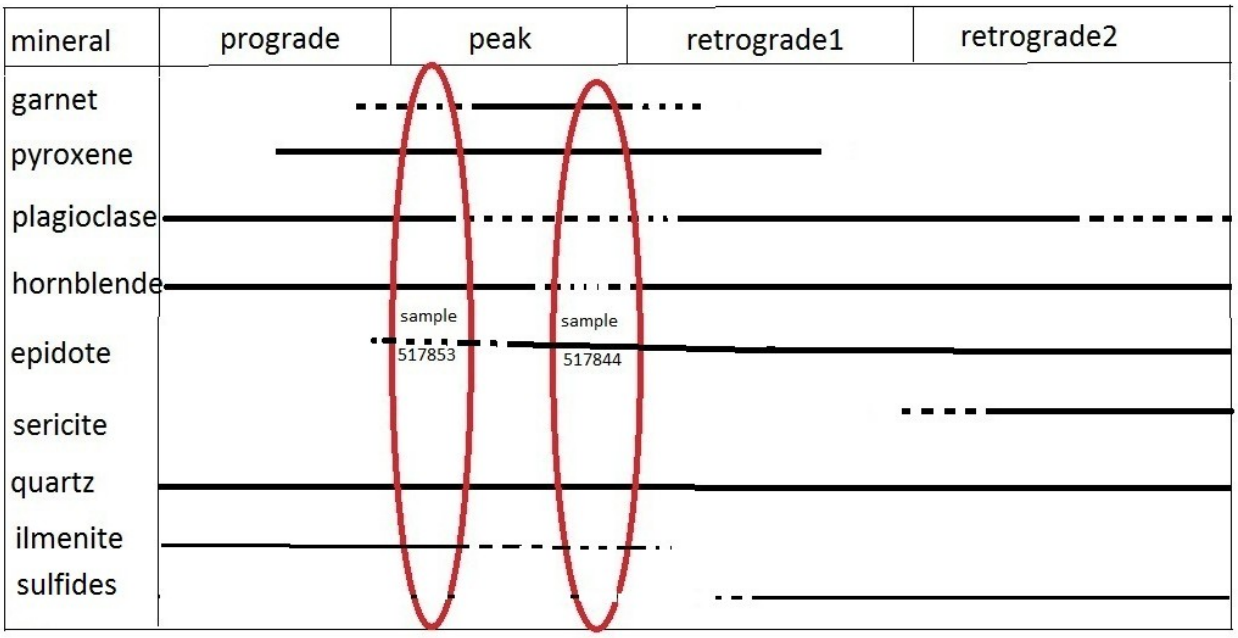

The variation in the textures and mineral abundance across sample 517855 is used to reveal the metamorphic history in the hydrothermal alteration zone (Table 4).The abundance of sericite, sulfides and quartz in layer 3 (Fig. 9f) suggest an alteration characterized by the infiltration of fluids that are enriched in potassium, sulfur and silica. This layer is interpreted as the mesosome. The geochemical influx significantly reduces the melting potential of these domains such that the altered rocks will start to melt at a much lower temperatures compared to the unaltered rocks during prograde metamorphism. Partial melting probably occurred in 2 stages. The first stage involved the generation of melts through dehydration melting of muscovite. This process occurred at a much lower temperature (600^{Θ} C) while a second stage of partial melting that involved the dehydration melting of hornblende occurred at a higher temperature (650^{Θ} C). A possible reaction for these 2 stages is as follows:

1). Muscovite + quartz = hornblende + K feldspar component and albite component (melt)

2). Hornblende + Quartz = clinopyroxene + plagioclase + melt

The breakdown of muscovite in the presence of quartz provides the source of k feldspar component present in the melt. The quartzo-feldspathic veins (Fig. 9c) probably represent the crystallization of the melt and are interpreted as the neosome. The unaltered clinopyroxene in layer 2 (Fig. 9d) that occur interstitial to quartz veins probably represent a residue of partial melting and this layer is interpreted as the melanosome.

Both the quartzo-feldspathic vein and the interstitial clinopyroxene are not altered suggesting that partial melting postdate hydrothermal alteration. The dominant sulfide that occurs in the hydrothermal alteration assemblage is pyrrhotite. A possible equation for the formation of pyrrhotite can be expressed as follows

Arsenopyrite + pyrite = melt + pyrrhotite

The replacement of pyrrhotite by magnetite and pyrite suggests atmospheric weathering whereby the ore is being oxidized.

Table 4. Metamorphic events and variation in relative abundance of mineral phases in the hydrothermal alteration zone (Pl= plagioclase; Hbl= hornblende; Cpx= clinopyroxene; Qtz= quartz; Musc= muscovite; Ep= epidote; K-fsp= K feldspar; Bt= biotite; Py= pyrite; Po= pyrite; Ccp= chalcopyrite; Mag = magnetite; Hem = hematite).

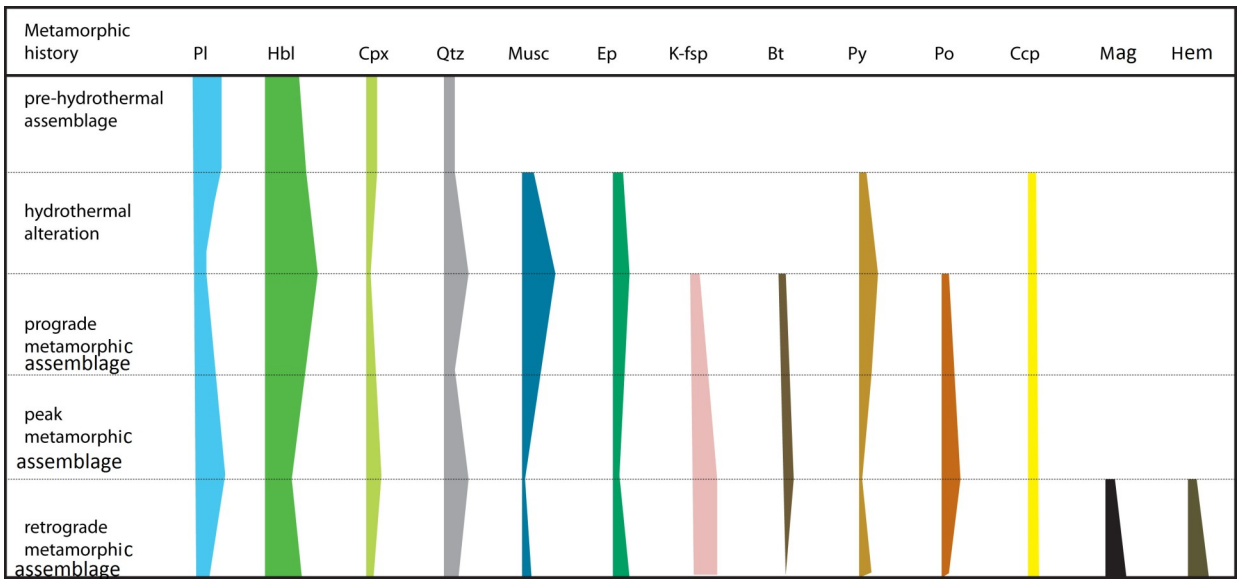

8. Model for partial melt formation in the hydrothermal alteration zone

Based on PT pseudosection and observed mineral sequence in the hydrothermal alteration zones and the following model is predicted for the formation of partial melt in a system containing plagioclase, muscovite, quartz, hornblende and, clinopyroxene.

For pressures less than 10000 bar, partial melting is strongly dependent on temperatures. With increase in temperature, muscovite is dehydrated and melts will start to form at temperatures of 873 k.

Table 5. Predicted phase composition at 900 k, 4000 bar

Phases	Wt. %	Vol. %	Mol. %
Melt	2.60	3.80	9.21
Feldspar	44.42	48.26	61.02
Amphibole	46.98	46.93	20.00
Clinopyroxene	5.98	5.07	9.77

Table 6. Predicted phase composition at 973 k, 4000 bar

Phases	Wt. %	Vol. %	Mol. %
Melt	7.70	10.50	18.45
Feldspar	42.63	45.91	46.94
Amphibole	32.34	29.64	11.17
Clinopyroxene	13.55	11.49	17.91
Orthopyroxene	3.73	2.46	5.52

Generally, as temperature increases, the more hydrous mineral phases decrease in abundance and there is a corresponding increase in the abundance of melt and anhydrous mineral phases (Table 5 & 6).

Garnet is uncommon for preasure less than 4500 bar in a MnO-poor system.

9. Conclusion

Petrography and mineralogy carried out during this study has led to the following conclusions.

1. Magmatic stage during which cumulate textures observed in ultramafic rocks was formed.
2. An eclogite facies metamorphism during which in situ partial melt pockets were formed in mafic rocks.
3. A low grade fluid present (greenschist) metamorphic event during which sulfide mineralization took place.
4. An upper amphibolites facies metamorphism during which the hydrothermal alteration assemblages were partially molten to form the quartzo-feldspathic veins and clinopyroxene
5. Supergene overprint during which pyrite was exsolved from pyrrhotite and the deposition of hematite around sulfides.

10. Acknowledgements

I would like to thank my supervisor Dr. Anders Schersten for his invaluable support and more especially, his kind words of encouragement. Special thanks go to my Co-supervisor Dr. Jochen Kolb for providing me with samples and insights throughout the work of this thesis. Thanks to Dr. Alfons Berger and the Geological Institute of the University of Copenhagen for giving me the opportunity to use their laboratory. Thanks to Prof. Charlotte Möller, Prof. James Connolly for clarification on thermobarometry, Prof. Anders Lindh for help with SEM analysis and Karolina Bjärnborg for helping out with Ore microscopy.

Special thanks also go to my wife Mshie Emidee née Tebi and kids for all their prayers, love and always being there for me.

I want to acknowledge the following friends Samuel Kometa, Serge Nzoke Baman, Mukumu Emmanuel, Herbert Mbufong, Tomas Ohman and Debora Enongene for their support and friendship during my stay in Sweden.

11. References

Bonnet, A-L. & Corriveau, L., 2007: Alteration vector to metamorphosed hydrothermal systems in gneissic terranes. *Mineral deposits of Canada* 5, 1035-1049.

Connolly, J. A. D., Memmi, I., Trommsdorff, V., Franceshelli, M. & Ricci, C. A., 1994: Forward modeling of calc-silicate microinclusions and fluid evolution in a graphitic metapelite (NE Sardinia). *American Mineralogist* 79, 960–972.

Connolly, J. A. D., Petrini, K., 2002: An automated strategy for calculation of phase diagram sections and retrieval of rock properties as a function of physical conditions. *Journal of Metamorphic Geology* 20, 697-708.

Friend, C. R. L. & Nutman, A. P., 2001: U-Pb zircon study of tectonically bounded blocks of 2940-2840 Ma crust with different metamorphic histories, Paamiut region, South-West Greenland: implications for the tectonic assembly of the North Atlantic craton. *Precambrian Research* 105, 143-164.

Frost, B. R., Mavrougenes, J. A., 2002: Partial melting of sulfide ore deposits during medium-and high-grade metamorphism. *The Canadian Mineralogist* 40, 1-15.

Garcia-Casco, A., Lazaro, C., Rojas-Agramonte, Y., Kroner, A., Torres-Roldan, R., Neubauer, F., Nunez, K., Millan, G., Blanco-Quinero, I., 2008: Partial Melting and Counter clockwise PT Path of Subducted Oceanic Crust (Sierra del Convento Melange, Cuba). *Journal of Petrology* 49, 129-161

Ineson, P. R., 1989: Introduction to practical ore microscopy. Longman Earth science series

Kishida, A. & Kerric, R., 1987: Hydrothermal alteration zoning and gold concentration at the Ker-Adison Archean lode gold deposit, Kirkland Lake, Ontario. *Economic Geology* 82, 649-690.

Kolb, J., 2011: Controls of hydrothermal quartz vein mineralization and wall rock alteration in the Paamiut and Tartoq area, South-West Greenland. *Geological Survey of Denmark and Greenland Report 10*.

McFarlane, C.R.M., 2006: Palaeoproterozoic evolution of the Challenger Au deposit, South Australia, from monazite geochronology. Journal *of Metamorphic Geology* 24, 75-87.

McCuaig, T. C., Kerrich, R., 1998: P-T–t deformation fluid characteristics of lode-gold deposits: evidence from alteration systematic. *Ore Geology Review* 12, 381-453.

McGregor, V.R. & Friend, C. R. L., 1997: Field recognition of rocks totally retrogressed from granulite facies: An example from Archean rocks in the Paamiut region, South-West Greenland. *Precambrian Research* 86, 59-70.

Phillips, G. N. & Powell, R., 2009: Formation of gold deposits: Review and evaluation of the continuum model. *Earth Science Review* 94, 1-21.

Phillips, G. N. & Powell, R., 2010: Formation of gold deposits: A metamorphic devolitilization model. *Journal of metamorphic Geology* 28, 689-718.

Ramdohr, P., 1969: The Ore minerals and their intergrowth. Pergamon Press.

Steenfelt, A., Garde, A. A. & Moyen, J.-F., 2005: Mantle wedge involvement in the petrogenesis of Archaean grey gneisses in West Greenland. *Lithos* 79, 207–228.

Stuewe, K. & Powell, R., 1995: PT paths inferred from modal proportions: Application to the Koralm Complex, Eastern Alp. *Mineralogy and*

Petrology 119, 83–93.
Tindle, A. G. & Webb, P. C., 1994: PROBE-AMPH- a spreadsheet program to the classify microprobe-derived amphibole analyses. Journal *of Computers & Geoscience* 20, Issue 7-8.
Tomkins, A. G. & Grundy, C., 2009: Upper temperature Limits of Orogenic Gold Deposit Formation: Constraints from the Granulite-Hosted Griffin`s Find deposit, Yilgarn Craton. *Economic Geology* 104, 669-685.
Windley, B. F., Garde A. A., 2008: Arc-generated blocks with crustal sections in the North Atlantic craton of West Greenland: Crustal growth in the Archean with modern Analogues. *Earth-Science Reviews* 93
Winkler, G. F., 1976: Petrogenesis of Metamorphic Rocks. Springer–Verlag, fifth edition.
Winter, J. D., 2001: Principles of Igneous and Metarmorphic Petrology. Prentice Hall, 2nd edition, 477-600.

Appendix 1: BUILD file (Connolly 1990) calculated using bulk composition for sample 517855

```
hp02ver.dat     thermodynamic data file
no_print | print generates print output
plot     | no_plot suppresses plot output
solution_model.dat       solution model file, blank = none
hydrothermal alteration
perplex_option.dat     computational option file
   5 calculation type: 0 - composition, 1 - Schreinemakers, 3 - Mixed, 4 - gwash, 5 - gridded min, 7 - 1d fract, 8 - gwash 9 - 2d fract, 10 - 7 w/file input
   0 unused place holder, post 06
   0 unused place holder, post 06
   0 unused place holder, post 06
   0 unused place holder, post 06
   0 unused place holder, post 06
   0 unused place holder, post 06
   0 unused place holder, post 06
   0 unused place holder, post 06
   0 unused place holder, post 06
   0 number component transformations
  15 number of components in the data base
   1 component amounts, 0 - molar, 1 weight
   0 unused place holder, post 06
   0 unused place holder, post 06
   0 unused place holder, post 05
   5 ifug EoS for saturated phase
   2 gridded minimization dimension (1 or 2)
   0 special dependencies: 0 - P and T independent, 1 - P(T), 2 - T(P)
 0.00000        0.00000        0.00000        0.00000        0.00000     Geothermal gradient polynomial coeffs.

begin thermodynamic component list
NA2O  1  1.27000       0.00000        0.00000        weight amount
MGO   1  4.65000       0.00000        0.00000        weight amount
AL2O3 1  12.8600       0.00000        0.00000        weight amount
K2O   1  1.29000       0.00000        0.00000        weight amount
CAO   1  10.0000       0.00000        0.00000        weight amount
FEO   1  7.60000       0.00000        0.00000        weight amount
H2O   1  1.00000       0.00000        0.00000        weight amount
end thermodynamic component list

begin saturated component list
SIO2  1  57.8100       0.00000        0.00000        weight amount
end saturated component list

 begin saturated phase component list
end saturated phase component list

 begin independent potential/fugacity/activity list
end independent potential list

 begin excluded phase list
end excluded phase list

begin solution phase list
Pheng(HP)
feldspar
Cpx(HP)
pMELTS(G)
GlTrTsPg
end solution phase list

 8000.0        1073.0        0.00000000  0.0000        0.0000  max p, t, xco2, u1, u2
 3000.0        573.00        0.00000000  0.0000        0.0000  min p, t, xco2, u1, u2
 0.0000        0.0000        0.00000000  0.0000        0.0000  unused place holder post 06

 2  1  4  5  3    indices of 1st & 2nd independent & sectioning variables
```

Appendix 2: BUILD file (Connolly 1990) calculated

```
using bulk composition for sample 517844


hp02ver.dat     thermodynamic data file
no_print | print generates print output
plot     | no_plot suppresses plot output
solution_model.dat     solution model file, blank =
none
garnet bearing sample(517844)
perplex_option.dat     computational option file
    5 calculation type: 0 - composition, 1 -
Schreinemakers, 3 - Mixed, 4 - gwash, 5 - gridded
min, 7 - 1d fract, 8 - gwash 9 - 2d fract, 10 - 7 w/file
input
    0 unused place holder, post 06
    0 unused place holder, post 06
    0 unused place holder, post 06
    0 unused place holder, post 06
    0 unused place holder, post 06
    0 unused place holder, post 06
    0 unused place holder, post 06
    0 unused place holder, post 06
    0 unused place holder, post 06
    1 number component transformations
   15 number of components in the data base
FE2O3 13 component transformation
  0.00   0.00   0.00   0.00   0.00   0.00   0.00   0.00
2.00   0.00   0.00   0.00   0.50
  0.00   0.00
    1 component amounts, 0 - molar, 1 weight
    0 unused place holder, post 06
    0 unused place holder, post 06
    0 unused place holder, post 05
    5 ifug EoS for saturated phase
    2 gridded minimization dimension (1 or 2)
    0 special dependencies: 0 - P and T independent, 1 -
P(T), 2 - T(P)
 0.00000      0.00000      0.00000      0.00000
0.00000     Geothermal gradient polynomial coeffs.

begin thermodynamic component list
MGO   1  3.39000      0.00000      0.00000     weight
amount
AL2O3 1  12.6300      0.00000      0.00000     weight
amount
CAO   1  12.3100      0.00000      0.00000     weight
amount
FE2O3 1  1.60000      0.00000      0.00000     weight
amount
FEO   1  13.7000      0.00000      0.00000     weight
amount
end thermodynamic component list

begin saturated component list
SIO2  1  52.5900      0.00000      0.00000     weight
amount
end saturated component list

begin saturated phase component list
H2O
end saturated phase component list

begin independent potential/fugacity/activity list
end independent potential list

begin excluded phase list
end excluded phase list

begin solution phase list
Ep(HP)
Cpx(HP)
Gt(HP)
GlTrTsPg
end solution phase list

 30000.0      1373.0     0.00000000  0.0000      0.0000
max p, t, xco2, u1, u2
 10000.0      573.00     0.00000000  0.0000      0.0000
min p, t, xco2, u1, u2
 0.0000      0.0000     0.00000000  0.0000      0.0000
unused place holder post 06

 2  1  3  4  5   indices of 1st & 2nd independent &
sectioning variables
```

Appendix 3: Whole rock geochemistry

Nr.		517841	517842	517843	517844	517845	517846	517847	517848	517849	517850	517851	517852	517853	517854	517855	517856	517857	517858	517859	517860	517861	517862	517863	517864	517865
		Leuco-granite	meta-gabbro	quartz vein	amphibolite	meta-rhyolite	Leuco-granite	amphibolite	quartz vein	quartz vein	meta-gabbro	meta-gabbro	quartz vein	amphibolite	peridotite	meta-gabbro	meta-gabbro	TTG gneiss	meta-rhyolite	quartz vein	peridotite	peridotite	peridotite	peridotite	quartz vein	amphibolite
alteration			melt pocket		melt pocket	melt pocket			melted alteration		sulphides	sulphides		melt pocket		sulphides	sulphides		proximal							alteration
SiO2	(wt.%)	76.05	48.74		52.59	66.76	75.80	52.50			43.76	50.88		52.22	45.12	57.81	53.07	68.91	67.43		52.16	52.23		44.22		51.72
TiO2		0.022	0.753		1.325	0.488	0.008	1.513			1.390	1.202		1.004	0.282	0.776	0.898	0.533	0.450		0.354	0.252		0.245		1.131
Al2O3		13.67	15.30		12.63	15.06	14.40	13.21			12.57	9.63		8.39	8.82	12.85	13.50	15.10	15.14		3.90	4.33		5.14		14.11
Fe2O3		0.46	12.18		15.33	3.93	0.31	17.93			22.42	20.00		16.78	10.34	8.55	9.95	3.63	4.39		9.29	8.40		9.94		15.39
FeO					13.79									15.09		7.69										
MnO		0.003	0.206		0.262	0.058	0.001	0.241			0.162	0.315		0.261	0.165	0.151	0.173	0.043	0.058		0.140	0.133		0.159		0.222
MgO		0.11	7.35		3.39	1.40	0.05	4.50			3.39	6.07		7.36	21.66	4.65	5.45	1.11	1.73		21.74	23.23		27.04		5.29
CaO		1.58	11.43		12.31	2.91	2.58	8.07			7.44	9.58		12.59	7.75	10.00	10.78	2.56	3.91		9.16	6.80		7.10		8.90
Na2O		3.86	1.32		0.99	4.22	5.47	2.26			1.64	1.75		1.41	0.76	1.27	1.23	4.27	3.36		0.37	0.26		0.48		2.98
K2O		3.60	1.12		0.21	2.38	0.15	0.26			0.80	0.18		0.16	0.08	1.29	1.54	2.99	1.48		0.55	1.22		0.05		0.37
P2O5		0.01	0.06		0.02	0.11	< 0.01	0.13			0.12	0.09		0.09	0.03	0.05	0.09	0.20	0.12		0.03	0.02		< 0.01		0.08
LOI		0.36	1.55		0.60	1.38	0.37	0.02			5.39	0.80		0.47	4.48	2.73	2.97	0.75	1.19		3.08	3.58		5.74		0.57
Total		99.73	100.01		113.45	98.70	99.14	100.63			99.08	100.50		115.83	99.49	107.82	99.65	100.10	99.26		100.77	100.46		100.11		100.76
TOT/S																										
TOT/C																										
Cr	(ppm)	80	241		15	37	50	10			14	26		141	1850	53	50	18	44		1190	1140	2130	1550		81
Ni		< 20	110		50	20	< 20	50			50	40		140	800	40	60	< 20	< 20		1110	1160	2320	1150		70
Co		< 1	52		41	10	< 1	52			46	34		74	76	30	36	8	4		84	77	97	92		39
Sc		< 1	46.6		42.9	6.6	< 1	50.1			47.6	33.9		30.6	26.0	44.8	49.3	5.2	8.2		18.0	15.0		19.0		49.2
V		< 5	277		373	57	< 5	435			410	293		230	151	284	329	46	63		89	72		108		371
Cu		< 10	170		1290	30	< 10	140			850	50		260	< 10	260	330	30	40		270	210	70	50		90
Pb		30	< 5		5	15	68	< 5			7	6		6	< 5	15	15	21	7		< 5	< 5	< 5	< 5		< 5
Zn		< 30	100		180	160	< 30	150			90	210		130	70	210	240	70	80		80	80	60	70		130
Bi		< 0.1	0.6				< 0.1								0.2						0.4	0.3	0.4	0.4		
Sn		< 1	< 1		3	< 1	< 1	< 1			1	< 1		1	< 1	< 1	< 1	2	< 1		< 1	< 1	< 1	< 1		< 1
Cd																										
In		< 0.1	< 0.1		< 0.1	< 0.1	< 0.1	< 0.1			< 0.1	< 0.1		< 0.1	< 0.1	< 0.1	< 0.1	< 0.1	< 0.1		< 0.1	< 0.1	< 0.1	< 0.1		< 0.1
Tl		0.47	0.13		< 0.05	0.40	< 0.05	< 0.05			0.18	< 0.05		< 0.05	< 0.05	0.22	0.28	0.51	0.35		0.28	0.47	< 0.05	< 0.05		0.09
W		< 0.5	< 0.5		7.0	0.5	1.0	< 0.5			9.8	10.9		2.0	< 0.5	3.5	2.7	< 0.5	< 0.5		< 0.5	< 0.5	< 0.5	49.0		< 0.5
Mo		8	< 2		< 2	< 2	5	< 2			4	< 2		< 2	< 2	3	3	34	3		< 2	< 2	< 2	2		< 2
As		< 5	4.5		5.9	4.9	< 5	5.0			27.0	36.1		14.4	< 5	6.2	< 0.5	3.1	4.6		< 5	< 5	< 5	< 5		2.5
Se			< 3		< 3	< 3		< 3			< 3	< 3		< 3		< 3	< 3	< 3	< 3							< 3
Sb		< 0.2	< 0.2		0.3	< 0.2	< 0.2	< 0.2			0.6	0.5		0.7	< 0.2	< 0.2	< 0.2	< 0.2	< 0.2		< 0.2	< 0.2	< 0.2	< 0.2		< 0.2
Ag		< 0.5	< 0.5		0.9	0.8	< 0.5	0.7			0.8	0.8		0.9	< 0.5	0.8	0.8	1.6	0.7		< 0.5	< 0.5	< 0.5	< 0.5		< 0.5
Au	(ppb)		11	3	113	< 2		< 2	28	3	< 2	32	32	410	< 1	131	114	< 2	< 2	3	7	6	< 1	5	5	< 2
Pt															7.9						3.3	4.1	6.1	4.5		
Pd															6.7						5.1	5.4	5.5	4.3		
Ir	(ppm)		< 5		< 5	< 5		< 5			< 5	< 5		< 5		< 5	< 5	< 5	< 5							< 5
Hg																										
Rb		85	35		6	87	3	3			38	6		5	< 1	58	71	95	51		24	56	< 1	< 1		9
Cs		2.5	0.7		0.5	2.5	0.6	0.3			3.2	1.0		0.4	0.2	2.7	3.9	3.0	5.4		5.8	13.8	0.5	0.4		0.8
Ba		557	275		36	569	29	36			82	49		43	< 3	177	189	1052	309		20	41		9		96
Sr		252	98		350	274	227	216			88	164		344	40	85	101	495	219		27	21		92		113
Ga		19	19		22	22	20	23			22	15		13	8	18	19	25	18		6	7	7	6		16
Ge		1.1	2.3		2.5	1.2	1.2	2.3			1.7	2.0		2.1	1.5	1.8	1.8	1.3	1.5		2.6	2.3	1.4	1.7		1.8
Hf		1.1	1.3		2.6	2.7	1.2	2.7			2.7	1.8		1.7	0.3	1.4	1.7	5.6	2.7		0.6	0.4	0.5	0.4		1.9
Zr		36	52		105	128	30	108			117	75		71	13	56	68	276	109		24	14	18	16		75
Nb		1.5	2.6		4.4	4.2	0.7	4.0			4.7	3.6		3.9	0.3	2.7	3.8	11.7	4.8		1.9	1.9	1.5	1.0		2.7
Y		0.6	18.9		37.7	5.8	6.2	35.2			35.8	11.6		16.7	5.8	19.8	24.0	11.0	3.9		6.4	4.7	7.2	7.5		23.7
Th		0.64	0.59		0.83	2.72	6.60	0.69			0.87	0.82		0.65	0.16	0.46	0.75	13.50	2.38		0.15	0.14	0.14	0.22		0.50
U		0.67	0.48		0.45	0.63	2.31	0.43			1.30	0.50		0.25	0.28	0.18	0.21	2.30	0.81		9.42	6.43	0.10	0.09		0.14
La		0.62	3.89		9.15	19.40	2.50	2.90			5.58	3.01		5.55	0.82	3.20	5.12	66.90	8.22		1.57	1.01	2.04	1.82		2.85
Ce		1.20	9.86		18.60	37.70	7.03	12.70			15.80	7.57		15.20	1.86	8.65	13.10	128.00	14.40		4.38	2.87	3.56	4.27		8.95
Pr		0.10	1.33		2.41	4.19	0.61	1.78			2.30	1.09		2.16	0.27	1.23	1.80	13.00	1.61		0.62	0.39	0.46	0.57		1.38
Nd		0.32	6.49		11.00	15.40	2.24	9.85			11.10	5.57		10.60	1.32	6.21	8.48	42.60	6.47		2.91	1.92	1.97	2.72		7.32
Sm		0.08	2.04		3.58	2.60	0.69	3.53			3.72	1.89		3.03	0.49	2.05	2.66	5.82	1.16		0.92	0.63	0.61	0.86		2.52
Eu		0.315	0.800		1.520	0.688	0.367	1.210			1.040	0.613		1.020	0.179	0.721	0.868	1.250	0.378		0.215	0.151	0.181	0.251		0.778
Gd		0.10	2.78		5.36	1.90	0.85	5.64			5.63	2.53		3.76	0.91	3.03	3.90	3.26	0.88		1.35	0.97	0.92	1.29		3.87
Tb		0.02	0.51		1.00	0.26	0.15	1.00			1.02	0.42		0.61	0.17	0.56	0.69	0.41	0.13		0.23	0.17	0.17	0.23		0.69
Dy		0.09	3.38		6.42	1.26	0.94	6.32			6.22	2.41		3.42	1.07	3.49	4.30	2.20	0.81		1.36	0.98	1.18	1.39		4.33
Ho		0.02	0.74		1.36	0.23	0.20	1.34			1.29	0.47		0.64	0.23	0.74	0.91	0.42	0.17		0.26	0.19	0.25	0.28		0.91
Er		0.06	2.29		4.31	0.60	0.65	4.14			4.03	1.36		1.81	0.69	2.32	2.81	1.14	0.52		0.73	0.55	0.74	0.84		2.84
Tm		0.012	0.348		0.694	0.086	0.111	0.667			0.651	0.204		0.264	0.106	0.367	0.446	0.165	0.082		0.107	0.082	0.111	0.124		0.462
Yb		0.09	2.34		4.55	0.54	0.74	4.27			4.23	1.30		1.68	0.73	2.41	2.90	1.04	0.56		0.68	0.52	0.72	0.79		2.91
Lu		0.014	0.372		0.676	0.084	0.109	0.650			0.633	0.193		0.254	0.116	0.367	0.436	0.155	0.090		0.101	0.076	0.110	0.117		0.440
Ta		0.22	0.13		0.28	0.40	0.19	0.25			0.29	0.28		0.28	0.10	0.17	0.22	1.29	0.62		0.18	0.23	< 0.01	0.17		0.18
Be		1	< 1		< 1	< 1	2	< 1			< 1	< 1		< 1	< 1	< 1	< 1	1	2		< 1	< 1		< 1		< 1
Br			< 0.5		< 0.5	< 0.5		< 0.5			< 0.5	< 0.5		< 0.5		< 0.5	< 0.5	< 0.5	< 0.5							< 0.5
Li																										

Tidigare skrifter i serien "Examensarbeten i Geologi vid Lunds Universitet":

243. Hult, Elin, 2009: Oligocene to middle Miocene sediments from ODP leg 159, site 959 offshore Ivory Coast, equatorial West Africa. (15 hskp)
244. Olsson, Håkan, 2009: Climate archives and the Late Ordovician Boda Event. (15 hskp)
245. Wollein Waldetoft, Kristofer, 2009: Svekofennisk granit från olika metamorfa miljöer. (15 hskp)
246. Månsby, Urban, 2009: Late Cretaceous coprolites from the Kristianstad Basin, southern Sweden. (15 hskp)
247. MacGimpsey, I., 2008: Petroleum Geology of the Barents Sea. (15 hskp)
248. Jäckel, O., 2009: Comparison between two sediment X-ray Fluorescence records of the Late Holocene from Disko Bugt, West Greenland; Paleoclimatic and methodological implications. (45 hskp)
249. Andersen, Christine, 2009: The mineral composition of the Burkland Cu-sulphide deposit at Zinkgruvan, Sweden – a supplementary study. (15 hskp)
250. Riebe, My, 2009: Spinel group minerals in carbonaceous and ordinary chondrites. (15 hskp)
251. Nilsson, Filip, 2009: Föroreningsspridning och geologi vid Filborna i Helsingborg. (30 hskp)
252. Peetz, Romina, 2009: A geochemical characterization of the lower part of the Miocene shield-building lavas on Gran Canaria. (45 hskp)
253. Åkesson, Maria, 2010: Mass movements as contamination carriers in surface water systems – Swedish experiences and risks.
254. Löfroth, Elin, 2010: A Greenland ice core perspective on the dating of the Late Bronze Age Santorini eruption. (45 hskp)
255. Ellingsgaard, Óluva, 2009: Formation Evaluation of Interlava Volcaniclastic Rocks from the Faroe Islands and the Faroe-Shetland Basin. (45 hskp)
256. Arvidsson, Kristina, 2010: Geophysical and hydrogeological survey in a part of the Nhandugue River valley, Gorongosa National Park, Mozambique. (45 hskp)
257. Gren, Johan, 2010: Osteo-histology of Mesozoic marine tetrapods – implications for longevity, growth strategies and growth rates. (15 hskp)
258. Syversen, Fredrikke, 2010: Late Jurassic deposits in the Troll field. (15 hskp)
259. Andersson, Pontus, 2010: Hydrogeological investigation for the PEGASUS project, southern Skåne, Sweden. (30 hskp)
260. Noor, Amir, 2010: Upper Ordovician through lowermost Silurian stratigraphy and facies of the Borenshult-1 core, Östergötland, Sweden. (45 hskp)
261. Lewerentz, Alexander, 2010: On the occurrence of baddeleyite in zircon in silica-saturated rocks. (15 hskp)
262. Eriksson, Magnus, 2010: The Ordovician Orthoceratite Limestone and the Blommiga Bladet hardground complex at Horns Udde, Öland. (15 hskp)
263. Lindskog, Anders, 2010: From red to grey and back again: A detailed study of the lower Kundan (Middle Ordovician) 'Täljsten' interval and its enclosing strata in Västergötland, Sweden. (15 hskp)
264. Rääf, Rebecka, 2010: Changes in beyrichiid ostracode faunas during the Late Silurian Lau Event on Gotland, Sweden. (30 hskp)
265. Petersson, Andreas, 2010: Zircon U-Pb, Hf and O isotope constraints on the growth versus recycling of continental crust in the Grenville orogen, Ohio, USA. (45 hskp)
266. Stenberg, Li, 2010: Geophysical and hydrogeological survey in a part of the Nhandugue River valley, Gorongosa National Park, Mozambique – Area 1 and 2. (45 hskp)
267. Andersen, Christine, 2010: Controls of seafloor depth on hydrothermal vent temperatures - prediction, observation & 2D finite element modeling. (45 hskp)
268. März, Nadine, 2010: When did the Kalahari craton form? Constraints from baddeleyite U-Pb geochronology and geo-chemistry of mafic intrusions in the Kaapvaal and Zimbabwe cratons. (45 hp)
269. Dyck, Brendan, 2010: Metamorphic rocks in a section across a Svecnorwegian eclogite-bearing deformation zone in Halland: characteristics and regional context. (15 hp)
270. McGimpsey, Ian, 2010: Petrology and lithogeochemistry of the host rocks to the Nautanen Cu-Au deposit, Gällivare area,

northern Sweden. (45 hp)

271. Ulmius, Jan, 2010: Microspherules from the lowermost Ordovician in Scania, Sweden – affinity and taphonomy. (15 hp)
272. Andersson, Josefin, Hybertsen, Frida, 2010: Geologi i Helsingborgs kommun – en geoturistkarta med beskrivning. (15 hp)
273. Barth, Kilian, 2011: Late Weichselian glacial and geomorphological reconstruction of South-Western Scania, Sweden. (45 hp)
274. Mashramah, Yaser, 2011: Maturity of kerogen, petroleum generation and the application of fossils and organic matter for paleotemperature measurements. (45 hp)
275. Vang, Ina, 2011: Amphibolites, structures and metamorphism on Flekkerøy, south Norway. (45 hp)
276. Lindvall, Hanna, 2011: A multi-proxy study of a peat sequence on Nightingale Island, South Atlantic. (45 hp)
277. Bjerg, Benjamin, 2011: Metodik för att förhindra metanemissioner från avfallsdeponier, tillämpad vid Albäcksdeponin, Trelleborg. (30 hp)
278. Pettersson, Hanna, 2011: El Hicha – en studie av saltstäppssediment. (15 hskp)
279. Dyck, Brendan, 2011: A key fold structure within a Sveconorwegian eclogite-bearing deformation zone in Halland, south-western Sweden: geometry and tectonic implications. (45 hp)
280. Hansson, Anton, 2011: Torvstratigrafisk studie av en trädstamshorisont i Viss mosse, centrala Skåne kring 4 000 - 3 000 cal BP med avseende på klimat- och vattenståndsförändringar. (15 hp)
281. Åkesson, Christine, 2011: Vegetationsutvecklingen i nordvästra Europa under Eem och Weichsel, samt en fallstudie av en submorän, organisk avlagring i Bellinga stenbrott, Skåne. (15 hp)
282. Silveira, Eduardo M., 2011: First precise U-Pb ages of mafic dykes from the São Francisco Craton. (45 hp)
283. Holm, Johanna, 2011: Geofysisk utvärdering av grundvattenskydd mellan väg 11 och Vombs vattenverk. (15 hp)
284. Löfgren, Anneli, 2011: Undersökning av geofysiska metoders användbarhet vid kontroll av den omättade zonen i en infiltrationsdamm vid Vombverket. (15 hp)
285. Grenholm, Mikael, 2011: Petrology of Birimian granitoids in southern Ghana - petrography and petrogenesis. (15 hp)
286. Thorbergsson, Gunnlaugur, 2011: A sedimentological study on the formation of a hummocky moraine at Törnåkra in Småland, southern Sweden. (45 hp)
287. Lindskog, Anders, 2011: A Russian record of a Middle Ordovician meteorite shower: Extraterrestrial chromite in Volkhovian-Kundan (lower Darriwilian) strata at Lynna River, St. Petersburg region. (45 hp)
288. Gren, Johan, 2011: Dental histology of Cretaceous mosasaurs (Reptilia, Squamata): incremental growth lines in dentine and implications for tooth replacement. (45 hp)
289. Cederberg, Julia, 2011: U-Pb baddelyit dateringar av basiska gångar längs Romeleåsen i Skåne och deras påverkan av plastisk deformation i Protoginzonen (15 hp)
290. Ning, Wenxing, 2011: Testing the hypothesis of a link between Earth's magnetic field and climate change: a case study from southern Sweden focusing on the 1st millennium BC. (45 hp)
291. Holm Östergaard, Sören, 2011: Hydrogeology and groundwater regime of the Stanford Aquifer, South Africa. (45 hp)
292. Tebi, Magnus Asiboh, 2011: Metamorphosed and partially molten hydrothermal alteration zones of the Akulleq glacier area, Paamiut gold province, South-West Greenland. (45 hp)

LUNDS UNIVERSITET

Geologiska enheten
Institutionen för geo- och ekosystemvetenskaper
Sölvegatan 12, 223 62 Lund